

# Poincaré Invariant Three-Body Scattering at Intermediate Energies

T. Lin<sup>(a)</sup>, Ch. Elster<sup>(a,b)</sup>, W. N. Polyzou<sup>(c)</sup>, H. Witała<sup>(d)</sup>, and W. Glöckle<sup>(e)</sup>

*(a) Institute of Nuclear and Particle Physics, and Department of  
Physics and Astronomy, Ohio University, Athens, OH 45701, USA*

*(b) Physics Division, Argonne National Laboratory, Argonne, IL 60439, USA*

*(c) Department of Physics and Astronomy, The University of Iowa, Iowa City, IA 52242, USA*

*(d) M. Smoluchowski Institute of Physics, Jagiellonian University, PL-30059 Kraków, Poland and*

*(e) Institute for Theoretical Physics II, Ruhr-University Bochum, D-44780 Bochum, Germany*

(Dated: February 2, 2008)

The relativistic Faddeev equation for three-nucleon scattering is formulated in momentum space and directly solved in terms of momentum vectors without employing a partial wave decomposition. The equation is solved through Padé summation, and the numerical feasibility and stability of the solution is demonstrated. Relativistic invariance is achieved by constructing a dynamical unitary representation of the Poincaré group on the three-nucleon Hilbert space. Based on a Malfliet-Tjon type interaction, observables for elastic and break-up scattering are calculated for projectile energies in the intermediate energy range up to 2 GeV, and compared to their nonrelativistic counterparts. The convergence of the multiple scattering series is investigated as a function of the projectile energy in different scattering observables and configurations. Approximations to the two-body interaction embedded in the three-particle space are compared to the exact treatment.

PACS numbers: 21.45+v, 24.10.Jv, 25-10.+s

## I. INTRODUCTION

The lightest nuclei can be accurately modeled as systems of nucleons interacting via effective two- and three-body forces motivated e.g. by meson exchange. This picture is expected to break down at a higher energy scale, where the physics is more efficiently described in terms of subnuclear degrees of freedom. Few-body methods have been an essential tool for determining model Hamiltonians that describe low-energy nuclear physics. They also have the potential to be a useful framework for testing the limitations of viewing the nucleus as a few nucleon system. The latter requires extending few-body models and calculations to higher energies. In order to successfully do this, a number of challenges need to be addressed. These include replacing the nonrelativistic theory with a relativistic one, overcoming limitations imposed by interactions fit to elastic nucleon-nucleon (NN) scattering data, including new degrees of freedom that appear above the pion production threshold, as well as numerical problems related to the proliferation of partial waves characteristic for scattering calculations at higher energies. Thus the intermediate energy regime is a new territory for few-body calculations which waits to be explored.

In this paper we address two of the challenges. We demonstrate that it is now possible to perform converged three-body scattering calculations at energies up to 2 GeV laboratory kinetic energy. Key elements are a consistent implementation of a Poincaré symmetric quantum theory [1], and the use of direct integration methods that avoid the partial wave decomposition, successfully applied below the pion-production threshold [2]. In a series of publications [3, 4, 5] the technique of solving the nonrelativistic momentum-space Faddeev equation without partial waves has been mastered, for bound as well as scattering states. The relativistic Faddeev equation, based on a Poincaré invariant mass operator, has been formulated in detail in [6], showing that it has both kinematical and dynamical differences with respect to the corresponding nonrelativistic equation.

The formulation of the theory is given in a representation of Poincaré invariant quantum mechanics where the interactions are invariant with respect to kinematic translations and rotations [7]. The model Hilbert space is a three-nucleon Hilbert space (thus not allowing for absorptive processes). The method used to introduce the NN interactions in the unitary representation of the Poincaré group allows input of high-precision NN interactions [8, 9, 10] in a way that reproduces the measured two-body observables. However in this study we use a simpler, spin-independent interaction consisting of a superposition of an attractive and a repulsive Yukawa interaction that supports a bound state with the deuteron binding energy. This is mathematically equivalent to three-boson scattering. Poincaré invariance and  $S$ -matrix cluster properties dictate how the two-body interactions must be embedded in the three-body dynamical generators. Scattering observables are calculated using the Faddeev equation formulated with the mass Casimir operator (rest Hamiltonian) constructed from these generators. We want to point out that the relativistic Faddeev equation with realistic spin-dependent interactions has been solved below the pion-production threshold in a partial wave basis [11, 12, 13].

In order to estimate the size of relativistic effects the interactions employed in the nonrelativistic and relativistic calculations presented here are chosen to be two-body phase shift equivalent. This is achieved in this article by

adding the interaction to the square of the mass operator [14, 15]. Thus differences in relativistic and nonrelativistic calculations first appear in the three-body calculations. Those differences are in the choice of kinematic variables (Jacobi momenta are constructed using Lorentz boosts rather than Galilean boosts) and in the embedding of the two-body interactions in the three-body problem, which is a consequence of the non-linear relation between the two and three-body mass operators. These differences modify the permutation operators and the off-shell properties of the kernel of the Faddeev equation.

This article is organized as follows. In Section II the formulation of the Poincaré invariant Faddeev equation is given and numerical aspects for computing the Faddeev kernel are discussed. In Sections III and IV we present calculations for elastic and breakup processes in the intermediate energy regime from 0.2 to 1.5 GeV. Our focus here is the investigation of the convergence of the multiple scattering series as a function of projectile kinetic energy. We compare our calculations to selected breakup observables and investigate a simple approximation of the embedding of the two-body interaction into the three-body problem.

## II. SOLVING THE RELATIVISTIC FADDEEV EQUATION

A detailed formulation of Poincaré invariant three-body scattering has been given in [6], where the driving term in the relativistic Faddeev equation (first order in the two-body transition operator) has been used to evaluate cross sections for elastic as well as break-up scattering. This is now being complemented by fully solving the relativistic Faddeev equation based on the numerical techniques previously used to solve the non-relativistic Faddeev equation [3]. For the convenience of the reader essential equations are repeated, but for the detailed derivation of the expressions we refer to Ref. [6].

The symmetrized transition operators  $U(z)$  for elastic scattering and  $U_0(z)$  for breakup reactions can be expressed in terms of the solution  $T(z)$  of the symmetrized Faddeev equations

$$\begin{aligned} U(z) &= P(z - M_0) + PT(z) \\ U_0(z) &= (1 + P) T(z), \end{aligned} \quad (2.1)$$

where  $M_0$  is the invariant mass operator for three non-interacting particles and the permutation operator  $P$  is given by  $P = P_{12}P_{23} + P_{13}P_{23}$ . The operator  $T(z)$  is the solution to the symmetrized Faddeev equation

$$T(z) = T_1(z)P + T_1(z)P(z - M_0)^{-1}T(z). \quad (2.2)$$

where the operator  $T_1(z)$  is the two-body transition operator embedded in the three-particle Hilbert space and defined as the solution to

$$T_1(z) = V_1 + V_1(z - M_0)^{-1}T_1(z). \quad (2.3)$$

Here  $V_1 = V_{23} = M_{23} - M_0$  is the two-body interaction embedded in the three-body Hilbert space and  $M_{23}$  is the invariant mass operator for two interacting particles and a spectator.

For calculating transition matrix elements, explicit basis states need to be introduced. The momenta of the three particles can be labeled either by single-particle momenta  $\mathbf{p}_1$ ,  $\mathbf{p}_2$ , and  $\mathbf{p}_3$ , or the total momentum  $\mathbf{P}$  and the relativistic Poincaré-Jacobi momenta [6]  $\mathbf{q}$  and  $\mathbf{k}$ . The explicit relations between the three-body Poincaré Jacobi momenta and the single particle momenta are

$$\mathbf{q}_i = \mathbf{p}_i + \frac{\mathbf{P}}{M_0} \left( \frac{\mathbf{P} \cdot \mathbf{p}_i}{M_0 + \sqrt{M_0^2 + \mathbf{P}^2}} - \sqrt{m^2 + \mathbf{p}_i^2} \right). \quad (2.4)$$

Then the Poincaré-Jacobi momenta  $\mathbf{q}$  and  $\mathbf{k}$  are given as

$$\begin{aligned} \mathbf{q} &\equiv \mathbf{q}_i = -(\mathbf{q}_j + \mathbf{q}_k) \\ \mathbf{k} &\equiv \mathbf{k}_i = \mathbf{k}_{jk} = \frac{1}{2}(\mathbf{q}_j - \mathbf{q}_k) - \frac{1}{2}(\mathbf{q}_j + \mathbf{q}_k) \left( \frac{E_j - E_k}{E_j + E_k + \sqrt{(E_j + E_k)^2 - (\mathbf{q}_j + \mathbf{q}_k)^2}} \right), \end{aligned} \quad (2.5)$$

where  $E_i \equiv E(\mathbf{q}_i) = \sqrt{m^2 + \mathbf{q}_i^2}$ . In addition, the transformation from the single particle momenta  $\mathbf{p}_i$  to the Poincaré-Jacobi momenta has a Jacobian given by

$$|\mathbf{p}_1, \mathbf{p}_2, \mathbf{p}_3\rangle = \left| \frac{\partial(\mathbf{P}, \mathbf{k}, \mathbf{q})}{\partial(\mathbf{p}_1, \mathbf{p}_2, \mathbf{p}_3)} \right|^{1/2} |\mathbf{P}, \mathbf{k}, \mathbf{q}\rangle \quad (2.6)$$

where for  $\mathbf{P} = \mathbf{0}$  the Jacobian becomes

$$\left| \frac{\partial(\mathbf{P}, \mathbf{k}, \mathbf{q})}{\partial(\mathbf{p}_1, \mathbf{p}_2, \mathbf{p}_3)} \right|_{\mathbf{P}=\mathbf{0}}^{1/2} = \left( \frac{\sqrt{(E(\mathbf{q}_2) + E(\mathbf{q}_3))^2 - \mathbf{q}^2} (E(\mathbf{q}_2) + E(\mathbf{q}_3))}{4E(\mathbf{q}_2)E(\mathbf{q}_3)} \right)^{1/2}. \quad (2.7)$$

In the above expression we chose, without loss of generality, particle 1 as the spectator. The Poincaré-Jacobi momenta are relevant for the calculation of the permutation operator  $P$  in Eqs. (2.1) and (2.2). The matrix elements of the permutation operator are then explicitly calculated as

$$\begin{aligned} \langle \mathbf{k}', \mathbf{q}' | P | \mathbf{k}, \mathbf{q} \rangle = & N(\mathbf{q}', \mathbf{q}) \left[ \delta(\mathbf{k}' - \mathbf{q} - \frac{1}{2}\mathbf{q}' C(\mathbf{q}, \mathbf{q}')) \delta(\mathbf{k} + \mathbf{q}' + \frac{1}{2}\mathbf{q} C((\mathbf{q}', \mathbf{q}))) \right. \\ & \left. + \delta(\mathbf{k}' + \mathbf{q} + \frac{1}{2}\mathbf{q}' C(\mathbf{q}, \mathbf{q}')) \delta(\mathbf{p} - \mathbf{q}' - \frac{1}{2}\mathbf{q} C((\mathbf{q}', \mathbf{q}))) \right], \end{aligned} \quad (2.8)$$

where the function  $N(\mathbf{q}', \mathbf{q})$  contains the product of two Jacobians and reads

$$\begin{aligned} N(\mathbf{q}, \mathbf{q}') \equiv N(q, q', x') = & \frac{\sqrt{E(\mathbf{q}) + E(\mathbf{q} + \mathbf{q}')} \sqrt{E(\mathbf{q}') + E(\mathbf{q} + \mathbf{q}')}}{4E(\mathbf{q} + \mathbf{q}')} \\ & \times \frac{\sqrt[4]{(E(\mathbf{q}) + E(\mathbf{q} + \mathbf{q}'))^2 - \mathbf{q}^2} \sqrt[4]{(E(\mathbf{q}') + E(\mathbf{q} + \mathbf{q}'))^2 - \mathbf{q}^2}}{\sqrt{E(\mathbf{q})E(\mathbf{q}')}}. \end{aligned} \quad (2.9)$$

with  $x' = \hat{\mathbf{q}} \cdot \hat{\mathbf{q}}'$ . The function  $C(\mathbf{q}, \mathbf{q}')$  is calculated as

$$C(\mathbf{q}', \mathbf{q}) \equiv C(q', q, x') = 1 + \frac{E(\mathbf{q}') - E(\mathbf{q}' + \mathbf{q})}{E(\mathbf{q}') + E(\mathbf{q}' + \mathbf{q}) + \sqrt{(E(\mathbf{q}') + E(\mathbf{q}' + \mathbf{q}))^2 - \mathbf{q}^2}}. \quad (2.10)$$

These permutation operators, which change the order of coupling, are essentially Racah coefficients for the Poincaré group. In the nonrelativistic case the functions  $N(\mathbf{q}', \mathbf{q})$  and  $C(\mathbf{q}', \mathbf{q})$  both reduce to the constant 1 and have the relatively compact form of the matrix elements of  $P$  given in e.g. [3, 5].

In matrix form the Faddeev equation, Eq. (2.2), reads

$$\langle \mathbf{k}, \mathbf{q} | T | \varphi_d, \mathbf{q}_0 \rangle = \langle \mathbf{k}, \mathbf{q} | T_1 P | \varphi_d, \mathbf{q}_0 \rangle + \langle \mathbf{k}, \mathbf{q} | T_1 P (z - M_0)^{-1} T | \varphi_d, \mathbf{q}_0 \rangle, \quad (2.11)$$

where we have factored out a delta function in the total momentum and set  $\mathbf{P} = \mathbf{0}$ . Inserting complete sets of states and explicitly evaluating the permutation operator leads to

$$\begin{aligned} \langle \mathbf{k}, \mathbf{q} | T(W) | \varphi_d, \mathbf{q}_0 \rangle = & N(\mathbf{q}, \mathbf{q}_0) T_s \left( \mathbf{k}, \mathbf{q}_0 + \frac{1}{2}\mathbf{q} C(\mathbf{q}_0, \mathbf{q}), \mathbf{q}; \varepsilon \right) \varphi_d \left( \mathbf{q} + \frac{1}{2}\mathbf{q}_0 C(\mathbf{q}, \mathbf{q}_0) \right) \\ & + \int d^3 q' N(\mathbf{q}, \mathbf{q}') \frac{T_s(\mathbf{k}, \mathbf{q}' + \frac{1}{2}\mathbf{q} C(\mathbf{q}', \mathbf{q}), \mathbf{q}; \varepsilon) \langle \mathbf{q} + \frac{1}{2}\mathbf{q}' C(\mathbf{q}, \mathbf{q}'), \mathbf{q}' | T(W) | \varphi_d \mathbf{q}_0 \rangle}{W - \left( \sqrt{m^2 + \mathbf{q}^2} + \sqrt{m^2 + \mathbf{q}'^2} + \sqrt{m^2 + (\mathbf{q} + \mathbf{q}')^2} \right) + i\epsilon}. \end{aligned} \quad (2.12)$$

The quantities  $W$  and  $\mathbf{q}_0$  are determined by the laboratory kinetic energy  $E_{lab}$  of the incident nucleon,

$$W^2 = (m + m_d)^2 + 2m_d E_{lab}. \quad (2.13)$$

The nucleon rest mass is given by  $m$ , the rest mass of the deuteron is  $m_d = 2m - \varepsilon_d$ , where  $\varepsilon_d$  is the deuteron binding energy. The Poincaré Jacobi momentum between projectile and target,  $\mathbf{q}_0$ , is related to  $E_{lab}$  by

$$\mathbf{q}_0^2 = \frac{m_d^2 E_{lab}}{W^2} (E_{lab} + 2m). \quad (2.14)$$

The invariant parametric energy  $\varepsilon$  which enters the two-body t-matrix is given by  $\varepsilon = W - \sqrt{m^2 + \mathbf{q}^2}$ . Since we consider bosons, we introduce the symmetrized two-body transition matrix  $T_s$

$$\begin{aligned} T_s(\mathbf{k}, \mathbf{k}', \mathbf{q}; \varepsilon) = & T_1(\mathbf{k}, \mathbf{k}', \mathbf{q}; \varepsilon) + T_1(-\mathbf{k}, \mathbf{k}', \mathbf{q}; \varepsilon) \\ = & T_1(\mathbf{k}, \mathbf{k}', \mathbf{q}; \varepsilon) + T_1(\mathbf{k}, -\mathbf{k}', \mathbf{q}; \varepsilon). \end{aligned} \quad (2.15)$$

This two-body t-matrix has a simple pole at  $W = \sqrt{m^2 + \mathbf{q}^2} + \sqrt{m_d^2 + \mathbf{q}^2}$ . Thus, for the practical calculation we need to take this pole explicitly into consideration by defining

$$\begin{aligned}\hat{T}_s &= \left( W - \sqrt{m^2 + \mathbf{q}^2} - \sqrt{m_d^2 + \mathbf{q}^2} \right) T_s \\ \hat{T} &= \left( W - \sqrt{m^2 + \mathbf{q}^2} - \sqrt{m_d^2 + \mathbf{q}^2} \right) T.\end{aligned}\quad (2.16)$$

and solving Eq. (2.12) for  $\hat{T}$

$$\begin{aligned}&\langle \mathbf{k}, \mathbf{q} | \hat{T}(W) | \varphi_d, \mathbf{q}_0 \rangle \\ &= N(\mathbf{q}, \mathbf{q}_0) \hat{T}_s \left( \mathbf{k}, \mathbf{q}_0 + \frac{1}{2} \mathbf{q} C(\mathbf{q}_0, \mathbf{q}), \mathbf{q}; \varepsilon \right) \varphi_d \left( \mathbf{q} + \frac{1}{2} \mathbf{q}_0 C(\mathbf{q}, \mathbf{q}_0) \right) \\ &\quad + \int d^3 q' N(\mathbf{q}, \mathbf{q}') \frac{\hat{T}_s(\mathbf{k}, \mathbf{q}' + \frac{1}{2} \mathbf{q} C(\mathbf{q}', \mathbf{q}), \mathbf{q}; \varepsilon)}{W - \left( \sqrt{m^2 + \mathbf{q}'^2} + \sqrt{m_d^2 + \mathbf{q}'^2} \right) + i\epsilon} \\ &\quad \times \frac{\langle \mathbf{q} + \frac{1}{2} \mathbf{q}' C(\mathbf{q}, \mathbf{q}'), \mathbf{q}' | \hat{T} | \varphi_d \mathbf{q}_0 \rangle}{W - \left( \sqrt{m^2 + \mathbf{q}^2} + \sqrt{m^2 + \mathbf{q}'^2} + \sqrt{m^2 + (\mathbf{q} + \mathbf{q}')^2} \right) + i\epsilon}.\end{aligned}\quad (2.17)$$

For the explicit calculation we introduce the independent variables [3]

$$k = |\mathbf{k}|, \quad q = |\mathbf{q}|, \quad x_k = \hat{\mathbf{k}} \cdot \hat{\mathbf{q}}_0, \quad x_q = \hat{\mathbf{q}} \cdot \hat{\mathbf{q}}_0, \quad x_{kq}^{q_0} = (\hat{\mathbf{q}}_0 \times \hat{\mathbf{q}}) \cdot (\hat{\mathbf{q}}_0 \times \hat{\mathbf{k}}), \quad (2.18)$$

so that  $\langle \mathbf{k}, \mathbf{q} | \hat{T} | \varphi_d, \mathbf{q}_0 \rangle = \hat{T}(k, x_k, x_{kq}^{q_0}, x_q, q)$ , is a function of 5 variables. In the variables of Eq. (2.18) and defining  $y_{kq} = x_k x_q + \sqrt{1 - x_k^2} \sqrt{1 - x_q^2} x_{kq}^{q_0}$ , the final expression for Eq. (2.12) reads

$$\begin{aligned}&\hat{T}(k, x_k, x_{kq}^{q_0}, x_q, q) \\ &= N(q, q_0) \varphi_d \left( |\mathbf{q} + \frac{1}{2} \mathbf{q}_0 C(\mathbf{q}, \mathbf{q}_0)| \right) \\ &\quad \times \hat{T}_s \left( k, |\mathbf{q}_0 + \frac{1}{2} \mathbf{q} C(\mathbf{q}_0, \mathbf{q})|, y_{k, \mathbf{q}_0 + \frac{1}{2} \mathbf{q} C(\mathbf{q}_0, \mathbf{q})}; W - \sqrt{m^2 + \mathbf{q}^2} \right) \\ &\quad + \int d^3 q' N(q, q', x') \frac{\hat{T}_s \left( k, |\mathbf{q}' + \frac{1}{2} \mathbf{q} C(\mathbf{q}', \mathbf{q})|, y_{k, \mathbf{q}' + \frac{1}{2} \mathbf{q} C(\mathbf{q}', \mathbf{q})}; W - \sqrt{m^2 + \mathbf{q}^2} \right)}{W - \left( \sqrt{m^2 + \mathbf{q}'^2} + \sqrt{m_d^2 + \mathbf{q}'^2} \right) + i\epsilon} \\ &\quad \times \frac{\hat{T} \left( |\mathbf{q} + \frac{1}{2} \mathbf{q}' C(\mathbf{q}, \mathbf{q}')|, y_{\mathbf{q} + \frac{1}{2} \mathbf{q}' C(\mathbf{q}, \mathbf{q}'), q_0}, x_{\mathbf{q} + \frac{1}{2} \mathbf{q}' C(\mathbf{q}, \mathbf{q}'), q'}^{q_0}, y_{q' q_0}, q' \right)}{W - \left( \sqrt{m^2 + \mathbf{q}^2} + \sqrt{m^2 + \mathbf{q}'^2} + \sqrt{m^2 + (q^2 + q'^2 + 2qq'x')} \right) + i\epsilon}.\end{aligned}\quad (2.19)$$

While the deuteron pole can be numerically taken care of with a single subtraction in the  $q'$ -integration, the free three-nucleon propagator in the 2nd term under the integral of Eq. (2.19) contains singularities depending on  $q'$  as well as  $x'$  leading to a singular region in the  $q - q'$  plane. In order to simplify the calculation, we carry out the integration of the kernel in a frame in which the  $z$ -axis is along the direction of  $\mathbf{q}$ . In this frame  $x' = \hat{\mathbf{q}}' \cdot \hat{\mathbf{q}}$  and  $\phi'$  is the azimuthal angle of  $\mathbf{q}'$ . With these definitions one has

$$\begin{aligned}y_{q' q_0} &= x_q x' + \sqrt{1 - x_q^2} \sqrt{1 - x'^2} \cos(\phi_{q_0} - \phi') \\ y_{kq'} &= x_p x' + \sqrt{1 - x_k^2} \sqrt{1 - x'^2} \cos(\phi_k - \phi'),\end{aligned}\quad (2.20)$$

where  $\phi_k$  and  $\phi_{q_0}$  are the azimuthal angles of  $\mathbf{k}$  and  $\mathbf{q}_0$  in the frame described above. Since there is a freedom in choosing the  $x$ -axis, we may place  $\mathbf{q}_0$  in the  $xz$ -plane, this gives  $\phi_{q_0} = 0$ . With this choice  $\phi_k$  is evaluated as

$$\cos \phi_k = \frac{x_k - y_{kq} x_q}{\sqrt{1 - y_{kq}^2} \sqrt{1 - x_q^2}}. \quad (2.21)$$

The remaining variables in Eq. (2.19) are explicitly evaluated as

$$\begin{aligned}
|\mathbf{q} + \frac{1}{2}\mathbf{q}' C(\mathbf{q}, \mathbf{q}')| &= \sqrt{q^2 + \frac{1}{4}q'^2 C^2(q, q', x') + qq'x' C(q, q', x')} \\
|\mathbf{q}_0 + \frac{1}{2}\mathbf{q} C(\mathbf{q}_0, \mathbf{q})| &= \sqrt{q_0^2 + \frac{1}{4}q^2 C^2(q_0, q, x_q) + qq_0x_q C(q_0, q, x_q)} \\
|\mathbf{q}' + \frac{1}{2}\mathbf{q} C(\mathbf{q}', \mathbf{q})| &= \sqrt{q'^2 + \frac{1}{4}q^2 C^2(q', q, x') + qq'x' C(q', q, x')},
\end{aligned} \tag{2.22}$$

and

$$\begin{aligned}
y_{k, \mathbf{q}_0 + \frac{1}{2}\mathbf{q} C(\mathbf{q}_0, \mathbf{q})} &= \frac{\mathbf{k} \cdot (\mathbf{q}_0 + \frac{1}{2}\mathbf{q} C(\mathbf{q}_0, \mathbf{q}))}{k|\mathbf{q}_0 + \frac{1}{2}\mathbf{q} C(\mathbf{q}_0, \mathbf{q})|} \\
&= \frac{kq_0x_p + \frac{1}{2}kqy_{kq} C(q_0, q, x_q)}{k\sqrt{q_0^2 + \frac{1}{4}q^2 C^2(q_0, q, x_q) + qq_0x_q C(q_0, q, x_q)}} \\
y_{k, \mathbf{q}' + \frac{1}{2}\mathbf{q} C(\mathbf{q}', \mathbf{q})} &= \frac{\mathbf{k} \cdot (\mathbf{q}' + \frac{1}{2}\mathbf{q} C(\mathbf{q}', \mathbf{q}))}{k|\mathbf{q}' + \frac{1}{2}\mathbf{q} C(\mathbf{q}', \mathbf{q})|} \\
&= \frac{kq'y_{kq'} + \frac{1}{2}kqy_{kq} C(q', q, x')}{k\sqrt{q'^2 + \frac{1}{4}q^2 C^2(q', q, x') + qq'x' C(q', q, x')}} \\
y_{\mathbf{q} + \frac{1}{2}\mathbf{q}' C(\mathbf{q}, \mathbf{q}'), q_0} &= \frac{(\mathbf{q} + \frac{1}{2}\mathbf{q}' C(\mathbf{q}, \mathbf{q}')) \cdot \mathbf{q}_0}{q_0|\mathbf{q} + \frac{1}{2}\mathbf{q}' C(\mathbf{q}, \mathbf{q}')|} \\
&= \frac{qq_0x_q + \frac{1}{2}q'q_0y_{q_0q'} C(q, q', x')}{q_0\sqrt{q^2 + \frac{1}{4}q'^2 C^2(q, q', x') + qq'x' C(q, q', x')}}},
\end{aligned} \tag{2.23}$$

and

$$x_{\mathbf{q} + \frac{1}{2}\mathbf{q}' C(\mathbf{q}, \mathbf{q}'), q'}^{q_0} = \frac{y_{\mathbf{q} + \frac{1}{2}\mathbf{q}' C(\mathbf{q}, \mathbf{q}'), q'} - y_{\mathbf{q} + \frac{1}{2}\mathbf{q}' C(\mathbf{q}, \mathbf{q}'), q_0} y_{q_0 q'}}{\sqrt{1 - y_{\mathbf{q} + \frac{1}{2}\mathbf{q}' C(\mathbf{q}, \mathbf{q}'), q_0}^2} \sqrt{1 - y_{q_0 q'}^2}}, \tag{2.24}$$

with

$$\begin{aligned}
y_{\mathbf{q} + \frac{1}{2}\mathbf{q}' C(\mathbf{q}, \mathbf{q}'), q'} &= \frac{(\mathbf{q} + \frac{1}{2}\mathbf{q}' C(\mathbf{q}, \mathbf{q}')) \cdot \mathbf{q}'}{q'|\mathbf{q} + \frac{1}{2}\mathbf{q}' C(\mathbf{q}, \mathbf{q}')|} \\
&= \frac{qq'x' + \frac{1}{2}q'^2 C(q, q', x')}{q'\sqrt{q^2 + \frac{1}{4}q'^2 C^2(q, q', x') + qq'x' C(q, q', x')}}.
\end{aligned} \tag{2.25}$$

For the integration of the 3N propagator, each singularity in the  $x'$ -integration (for fixed  $q'$ ) is explicitly taken into account by a subtraction. However, this leads to logarithmic singularities in  $q'$  at the boundaries  $x' = \pm 1$ . These we integrate in the semi-analytic fashion introduced in Ref. [3] by using cubic Hermite splines. While using cubic Hermite splines is advantageous in dealing with the logarithmic singularities, this method is not as effective as Gauss-Legendre quadrature when integrating over large, non-singular regions. Thus, in order to make the most efficient use of both methods, we divide the interval of the  $q'$ -integration into several integration regions, and use Gauss-Legendre quadrature in the non-singular integrals, while keeping the cubic Hermite splines in the small regions around the singularities. With this procedure we are able to successfully integrate over the Faddeev kernel with sufficient accuracy. For the final solution of Eq. (2.19) the kernel is successively applied and the resulting terms are summed up as Padé sums. At the higher energies we will also carry out the Neumann sum.

Our explicit calculations are based on a simple interaction of Malfliet-Tjon type consisting of a superposition of an attractive and repulsive Yukawa interaction that supports a bound state with the deuteron binding energy. The parameters of this nonrelativistic interaction are given in Ref. [3]. In order to obtain a relativistic interaction which is phase shift equivalent with the nonrelativistic one, we employ a scheme in which  $4m$  multiplied with the interaction

is added to the square of the non-interacting two-body mass operator. This procedure was introduced by Coester, Pieper and Serduke [14] and used here in the form given in [15]. It guarantees that differences in the relativistic and nonrelativistic calculations first appear in the three-body calculations.

Before entering a detailed study on relativistic effects, we want to present further details on the numerical quality of our solution of the relativistic Faddeev equation. One internal consistency check of the solution is provided by the optical theorem, which states that the total cross section, being the sum of the total elastic cross section,  $\sigma_{el}$ , and the total breakup cross section,  $\sigma_{br}$ , must be equal to the imaginary part of the transition operator for elastic scattering  $U$  in forward direction. In the center-of-momentum (c.m.) frame this relation reads

$$\sigma_{el} + \sigma_{br} = \sigma_{tot} = -16\pi^3 \frac{E_n(q_0)E_d(q_0)}{q_0 W} \Im m(U(q_0, x=1)). \quad (2.26)$$

Listed in Table I are our fully relativistic calculations of the total cross sections for elastic scattering and breakup reaction for projectile energies from 0.1 to 2.0 GeV, together with the total cross sections. The total cross sections are calculated as sum of the elastic and breakup cross sections,  $\sigma_{tot}$ , and via the optical theorem,  $\sigma_{op}$ , from the imaginary part of the operator  $U$  in forward direction,  $x=1$ . A comparison of those two numbers for the total cross section shows, that our calculations fulfill the optical theorem to about 1% or better up to 1 GeV. This error increases to about 3% at 2 GeV. Here we did not push the calculations any further, since our model potential is too simple to take it to much higher energies anyway. For the sake of showing the numerical quality of our calculations, we included 2 GeV in Table I, but will not show any further observables at this energy.

The transition amplitude of Eq. (2.19) is a function of 5 variables, and is the solution of an integral equation in three dimensions. Thus, in the calculation the dependence of the result on the various choices of grids has to be considered. As far as the momentum grids are concerned, the accuracy of the calculation is most sensitive to the  $q$ -grid, as already found in Ref. [3]. In Fig. 1 we show the dependence of the relative error  $\Delta_q = \frac{\sigma_{op} - \sigma_{tot}}{\sigma_{op}} \times 100$  in the optical theorem as function of the size of the  $q$ -grid,  $N_q$ , for a calculation at 1 GeV projectile laboratory kinetic energy. The slope of  $\Delta_q$  shows that indeed the accuracy of the calculation is strongly influenced by the size of this grid. For our calculation,  $N_q = 50$  is sufficient at 1 GeV. Next, we consider the sensitivity of the calculation to the size of different angle grids. In Table II we give the cross sections for elastic scattering and breakup reactions together with the total cross section  $\sigma_{op}$  extracted from the optical theorem when varying the size of the different angle grids. We can see, that the results are most sensitive with respect to the grids in  $x_q$  and  $x'$ . It is common wisdom in calculations using an angular momentum basis that as the energy of the projectile increases, the number of partial waves needed to obtain a converged result increases rather quickly. In our 3D calculations, all partial waves are included. The increase in energy manifests itself in a two-body t-matrix acquiring a more pronounced peak structure in the forward and backward directions with respect to the angle between the two momentum vectors [17]. This peak structure at  $x_q = \pm 1$  must be adequately covered in calculations at higher energies to ensure converged results. In Fig. 2 we show the relative error  $\Delta_x = \frac{\sigma_{op} - \sigma_{tot}}{\sigma_{op}} \times 100$  in the optical theorem as function of the size of the  $x_q$ -grid for three different projectile laboratory kinetic energies. The necessity of increasing the  $x_q$ -grid with increasing projectile energy is clearly seen. Whereas for 0.2 GeV  $N_{x_q} = 24$  is clearly sufficient, at 0.5 GeV one needs already at least 28 points, whereas at 1 GeV a minimum of 36 points is required. This conclusion is also reached in our Table III, where we show the relativistic differential cross section at selected angles while varying the  $x_q$ -grid. It should be noted that the angle  $x_q$  is related to the angular momentum of the relative motion between the spectator and the interacting pair. The angle  $x_p$ , which is related to the angular momentum of the interacting pair is not nearly as sensitive as  $x_q$ . In Table II we vary the  $x_p$  grid from 20 to 24 points, and see hardly any difference.

It is illustrative to contrast the computational algorithm for direct integration with the experience gained when using a partial wave basis in the 3N system. Our experience tells us that at  $E_{lab} = 200$  MeV the total angular momentum of the 2N subsystem  $j$  needs to be  $j_{max} = 5$  to reach convergence. Furthermore, the maximum total angular momentum  $J$  of the 3N system required to reach convergence is  $J_{max} = 25/2$ . Let us assume that  $J_{max} = j_{max} + I_{max}$ , where  $I_{max} = s_i + \lambda$  is the maximal angular momentum of the projectile nucleon with respect to the target pair,  $s_i$  is the spin of the projectile and  $\lambda$  is the relative orbital angular momentum between the projectile and target pair. This leads to  $I_{max} = 15/2$  for a 3N scattering calculation at  $E_{lab} = 200$  MeV. Disregarding the spin degree of freedom for the three nucleons, leading to the three-boson model under consideration here, we find that  $J_{max} = 12$  with  $l_{max} = 5$  and  $\lambda_{max} = 7$  are necessary for a converged calculation at  $E_{lab} = 200$  MeV. In the three-boson case  $l$ , the orbital momentum of the interacting pair, and  $\lambda$  take the role of  $j$  and  $I$ .

In order to estimate the corresponding maximal number of angular momenta needed for  $E_{lab} = 1$  GeV, one needs the effective deuteron radius  $r_0$ , which leads to  $\lambda_{max} = 7$  at  $E_{lab} = 200$  MeV. Nonrelativistically the 3N c.m. energy is given as  $3/4 q_0^2 = 2/3 E_{lab}$ , leading to  $q_0 \simeq 400$  MeV/c at  $E_{lab} = 200$  MeV and  $q_0 \simeq 900$  MeV/c at  $E_{lab} = 1$  GeV. If we roughly set  $\lambda_{max} = q_0 \times r_0$ , then we find at  $E_{lab} = 200$  MeV a value  $r_0 \simeq 3.5$  fm, which appears reasonable. Applying the same value at  $E_{lab} = 1$  GeV then leads to  $\lambda_{max} = 15$ . Using our experience in calculating the NN system



in the GeV regime [18], where one needs for converged NN observables at least  $j_{max} = 14$  at 1 GeV, we estimate that a converged partial wave 3N calculation of the three-boson system would need  $J_{max} = l_{max} + \lambda_{max} = 14 + 15 = 29$ .

Let us now regard the two cases, (a)  $E_{lab} = 200$  MeV,  $l_{max} = 5$ ,  $\lambda_{max} = 7$ ,  $J_{max} = 12$ , and (b)  $E_{lab} = 1$  GeV,  $l_{max} = 14$ ,  $\lambda_{max} = 15$ ,  $J_{max} = 29$  in a partial wave decomposition. To illustrate the tremendous number of partial waves needed in (b) compared to the feasible case (a) it is sufficient to consider simple algebra for different values of  $J$ . Take for example  $J = 5$ . Then simple counting yields 30 different  $l - \lambda$  combinations in case (a) and 125 in case (b). For  $J = 10$  this number increases in case (b) to 160. Moreover, since the number of total  $J$ 's at 1 GeV is more than twice the number of  $J$ 's at 200 MeV, it appears quite unreasonable to enforce a partial wave decomposition at energies far above 200 MeV in the 3-boson (nucleon) system. In addition, it would also be numerically very demanding to evaluate the various ingredients in the Faddeev equation reliably for the very high angular momenta. Another advantage of using direct integration of vector variables in the Faddeev equation is the simplicity of the permutation operators.

### III. RESULTS AND DISCUSSION

In the following we present our results for elastic and breakup scattering in the energy regime from about 200 to 1500 MeV laboratory projectile kinetic energy. We start with a comparison of our model calculation to calculations based on a realistic NN force at lower energies in order to show that even though our model is very simple, we see similar features in the cross sections. Then we study relativistic effects at higher energies. There are several questions we want to address. First, we want to identify scattering observables that are sensitive to the difference between the relativistic and non-relativistic formulations of the three-body problems and to study the size of those relativistic effects as function of increasing energy. This can at present only be done with our model interaction. Second, we want to study the convergence properties of the Faddeev multiple scattering series as function of the projectile kinetic energy. Here the question of interest is, if, once the energy is high enough, it is sufficient to only consider the first few terms in the multiple scattering series. In addition, we also want to study some approximations to our relativistic scheme.

#### A. Comparison with calculations based on a realistic NN interaction at 200 MeV

The laboratory kinetic energy of 200 MeV is a perfect energy to study if the features of the 3N system we find based on our model interaction are also present in calculations based on a realistic model of the NN interaction, which describes the NN observables with high accuracy. The so-called high-precision interactions are fitted up to about 350 MeV, but strictly speaking only valid below the pion-production threshold. We also know [11, 12, 13] that relativistic effects are already visible at 200 MeV.

We choose the CD-Bonn interaction [9] for this comparison. In Fig. 3 we show the  $np$  total cross section extracted from the SAID database [19] together with the total cross section obtained from the MT-III interaction assuming bosonic symmetry. The parameters of the MT-III interaction [3] are adjusted such that a two-body bound state at  $E_d = 2.23$  MeV is supported. Fig. 3 shows that the experimental  $np$  total cross section falls slightly below the two-body cross section predicted by our model at energies smaller than  $E_{lab} \simeq 300$  MeV, is about equal between 300 and 400 MeV, and then reaches a constant value from about 600 MeV on, while our model prediction continues to decrease. The slight rise of the experimental value around 600 MeV is a manifestation of the influence of the  $\Delta(1232)$  resonance in the NN system. The CD-Bonn interaction is fitted to NN observables to about 350 MeV laboratory projectile energy and thus coincides with the SAID result up to that energy.

In Fig. 4 we show a comparison of elastic and breakup cross sections at 200 MeV projectile laboratory energy for the 3D calculations based on our MT-III model interaction and calculations based on a partial wave decomposition employing the CD-Bonn potential. The top row displays the differential cross section for elastic scattering. We see that in both cases the difference between the fully relativistic calculation and the nonrelativistic one is overall quite small, and mostly visible at the backward angles, an observation already made in [11]. The differential cross section in the forward direction is much larger for our model interaction, which is consistent with the larger two-body total cross section. In addition, there are more diffraction minima in the bosonic case than in the fermionic case, however, the minimum at around  $130^\circ$  is present in both calculations. In the middle row we display the cross section for inclusive breakup scattering as function of the laboratory kinetic energy of the ejected particle at fixed laboratory angle  $18^\circ$ . Both cross sections are qualitatively similar, the fully converged Faddeev calculation gives a lower cross section than the first order calculation, indicating the importance of rescattering contributions at this low energy. The difference between the relativistic and nonrelativistic calculations is quite small in both cases. In the calculation based on the CD-Bonn interaction the FSI peak is more pronounced due to the virtual bound state in the  $^1S_0$  state. The latter is absent in the MT-III model. The bottom row shows the five-fold differential cross section as function of the arc-length

$S$  for a configuration in which the laboratory angles  $\theta_1 = \theta_2 = 37^\circ$  are given in the scattering plane ( $\phi_{12} = 180^\circ$ ). The position of the peaks is identical for both calculations, which is a manifestation that peak structures are given by the kinematics of the problem. In both cases the relativistic calculation gives a significantly larger cross section for the central peak at  $S \approx 140$  MeV compared to the nonrelativistic result, an increase by a factor of  $\sim 1.5$  for the full partial wave calculation and by a factor  $\sim 2$  for the full 3D calculation. This increase is already present in both first order calculations. For the MT-III model this trend is the same for all other peaks, whereas for the CD-Bonn model the nonrelativistic calculations give a slightly larger cross section compared to the relativistic one in the peaks at small and large values of arc-length  $S$ .

Summarizing, the comparison of cross section obtained from our model interaction MT-III with those given by a realistic NN interaction like CD-Bonn at 200 MeV indicates that, despite our model being quite simple, the qualitative features of especially the breakup cross sections are very similar. The differences between the fully relativistic calculations and their nonrelativistic counterparts are still quite small at this low energy for elastic scattering and inclusive breakup. For the exclusive breakup, however, even at this energy complete configurations with large changes of the nonrelativistic cross section due to relativity can be found. This sensitivity of the complete breakup to relativistic effects has already been observed in [12, 13].

### B. Elastic Scattering at Intermediate Energies

Starting from our model interaction we now consider three-body scattering in the energy regime up to 1.5 GeV. The total cross section for elastic scattering is related to the symmetrized transition operator  $U$  of Eq. (2.1) via

$$\sigma_{el} = (2\pi)^4 \int d\Omega \frac{E_n^2(q_0) E_d^2(q_0)}{W^2} |\langle \varphi_d, \hat{\mathbf{q}}_0 | U | \varphi_d, \mathbf{q}_0 \rangle|^2. \quad (3.1)$$

In Fig. 5 we display the total cross section for elastic scattering as a function of the projectile kinetic energy up to 1.5 GeV obtained from our fully converged relativistic Faddeev calculation as well as the one obtained from the first order term. It is obvious that, especially for the energies below 300 MeV, the contribution of rescattering terms is huge. Since the logarithmic scale from the top panel is unsuited to extract detailed information about the size of relativistic effects, we show in the lower two panels the relative difference of the relativistic calculations with respect to their nonrelativistic counterparts. The bottom panel displays the relative difference between the relativistic first order term and its nonrelativistic counterpart as dotted line. Essentially the first order calculation does not show any effect. This is theoretically consistent when having in mind that in first order ( $T^{1st} = tP$ ) only the two-body t-matrix enters into the cross section. The relativistic two-body t-matrix is constructed to be phase-shift equivalent to the non-relativistic one via the CPS method [14, 15]. Thus, seeing no difference between the fully relativistic and the corresponding nonrelativistic calculations indicates that relativistic effects are taken into account consistently at the two-body level. Doing the same comparison with fully converged Faddeev calculations (solid line in the middle panel) indicates that relativistic effects in the three-body problem increase the elastic scattering total cross section with increasing energy. At our highest energy, 1.5 GeV, this increase is about 8.3%.

Often only effects due to relativistic kinematics are taken into account. Here we have the opportunity to study consequences of such a simple approximation. For the calculations labeled  $R_{kin}$  we only consider the Lorentz transformations from laboratory to center-of-momentum (c.m.) frame and the relativistic phase space factor of Eq. (3.1), whereas the matrix elements of the operator  $U$  are calculated from the solution of the nonrelativistic Faddeev equation. The relative difference between this calculation and a completely nonrelativistic calculation is indicated by the short-dashed line in the bottom panel of Fig. 5, where only the first order term is considered. The triple-dotted curve in the middle panel is the same comparison, but now between fully converged Faddeev calculations. For both, full and first order calculation, the effect is huge. To understand better which piece of the kinematics included is responsible for this large enhancement of the cross section, we also plot in Fig. 5 calculations (labeled  $NR_{cm}$ ), which only contain the Lorentz transformation between the laboratory and c.m. frame, but carry the nonrelativistic phase space factor in Eq. (3.1). The dash-dotted line in the lower panel show the 1st order calculation and the dotted line in the middle panel the full Faddeev calculation. Using a Lorentz transformation in the change of frames has the effect that the two-body t-matrix is calculated at a slightly different c.m. momentum  $\mathbf{q}_0$ , and thus there is a small effect, about a 5% underestimation of the total cross section. The huge effect is entirely due to the relativistic phase space factor, and relativistic dynamics then has an equally large effect of the opposite sign. This interplay of increasing effects due to the relativistic phase-space factor and decreasing effects due to relativistic dynamics has been already observed in the partial-wave based Faddeev calculations with realistic interactions [11]. It led for elastic scattering cross section at 250 MeV to relativistic effects which are relatively small and restricted to backward angles. Recent measurements of the neutron-deuteron ( $nd$ ) differential cross section at 248 MeV [16] indicate that for discrepancies of theoretical predictions in this observable, short range components of a three-nucleon force are equally important.



The problem with approximating relativistic effects only through kinematics and phase space factors can be easily understood in the 2+1 body problem, where the phase equivalence is achieved by choosing the invariant mass as a function of the non-relativistic two-body Hamiltonian,  $M = f(h)$ . The eigenvalues equation for the scattering problems

$$|\psi\rangle = \frac{1}{f(w) - f(h_0) + i0^+} (f(h) - f(h_0)) |\psi\rangle \quad |\psi\rangle = \frac{1}{w - h_0 + i0^+} (h - h_0) |\psi\rangle \quad (3.2)$$

are equivalent, but the replacement of  $f(w)$  by  $w$  must be compensated by replacing the interaction  $f(h) - f(h_0)$  by  $h - h_0$ . Including only kinematic relativistic effects is equivalent to making the replacement  $h_0 \rightarrow f(h_0)$  without making the compensating replacement  $v = h - h_0 \rightarrow f(h) - f(h_0)$ .

We also study a more sophisticated approximation to the relativistic dynamics. In Ref. [6] we described in detail how we obtain the transition amplitude of the 2N subsystem,  $T_1(\mathbf{k}, \mathbf{k}', \mathbf{q}; z) \equiv \langle \mathbf{k} | T_1(\mathbf{q}; z) | \mathbf{k}' \rangle$ , embedded in the three-particle Hilbert space which enters the Faddeev equation, Eq. (2.11). The fully off-shell amplitude is the solution of a first resolvent type equation [15] given by

$$\langle \mathbf{k} | T_1(\mathbf{q}; z) | \mathbf{k}' \rangle = \langle \mathbf{k} | T_1(\mathbf{q}; z') | \mathbf{k}' \rangle - \int d\mathbf{k}'' \langle \mathbf{k} | T_1(\mathbf{q}; z) | \mathbf{k}'' \rangle \left( \frac{1}{z - \sqrt{4(m^2 + \mathbf{k}''^2) + \mathbf{q}^2}} - \frac{1}{z' - \sqrt{4(m^2 + \mathbf{k}''^2) + \mathbf{q}^2}} \right) \langle \mathbf{k}'' | T_1(\mathbf{q}; z') | \mathbf{k}' \rangle. \quad (3.3)$$

Here  $T_1(z')$  is taken to be right half-shell with  $z' = \sqrt{4(m^2 + \mathbf{k}'^2) + \mathbf{q}^2} + i\epsilon$ . Note that in this equation the unknown matrix element is to the *left* of the kernel. It was suggested in Ref. [15] that a reasonable approximation to this embedded 2N transition amplitude might be the Born term of the above integral equation, which is

$$\langle \mathbf{k} | T_1^H(\mathbf{q}; z) | \mathbf{k}' \rangle \simeq \langle \mathbf{k} | T_1(\mathbf{q}; z') | \mathbf{k}' \rangle. \quad (3.4)$$

In this approximation, the fully off-shell 2N transition amplitude is replaced by a half-shell amplitude. The effect of this approximation is not large in elastic scattering, as shown in Fig. 6, where we plot the differential cross section in forward direction for the fully relativistic calculations and the ones containing the approximation of Eq. (3.4) to the boost (curves labeled H). Consistently and independent of projectile energy, approximating the embedded two-body t-matrix by the half-shell t-matrix leads to an underprediction of the differential cross section in forward direction. Though not plotted, this also leads to a smaller total cross section for elastic scattering.

Finally, we want to investigate the convergence of the multiple scattering series as a function of the projectile laboratory kinetic energy. One might expect that with increasing energy only a few terms in the multiple scattering series are sufficient for a converged result. Our converged relativistic Faddeev calculations now allow a detailed study. This is of particular interest, since recently relativistic calculations in the energy regime around 1 GeV have been published [20, 21, 22], which are carried out in a multiple scattering expansion of the Faddeev equations up to 2nd order, and which use the off-shell continuation of the experimental NN amplitudes as two-body input.

First we want to consider the convergence of the Faddeev multiple scattering series in the total cross sections for elastic scattering as well as breakup reactions as a function of projectile kinetic energy. In the bottom row of Fig. 7 the different orders (successively summed up as Neumann sum to the order indicated in the legend) are shown as functions of the projectile laboratory energy. We see a distinct difference in the behavior of the elastic total cross section in comparison with the breakup total cross section. While the elastic total cross section converges very rapidly, the total breakup cross section does not. The left upper panel of Fig. 7 shows the elastic total cross section as a function of the order in the multiple scattering series (the orders are successively summed up the one indicated on the x-axis). Even at 200 MeV there is very little change due to contributions from the 2nd or higher order rescattering terms. For the higher energies, the 1st order term already captures the essential physics. This is very different for the total breakup cross section, where for 200 MeV projectile energy the full solution of the Faddeev equation is clearly necessary. For energies of 1 GeV and higher, at least one rescattering contribution (2nd order in the multiple scattering series) is necessary to come close to the full solution.

Since the total cross section for elastic scattering might be insensitive to higher orders in the Faddeev multiple scattering series, we plot in Fig. 8 the differential cross section at forward and backward angles as a function of the order in the multiple scattering series for the same laboratory projectile energies. Here we see that at the lowest energy, 0.2 GeV, the convergence is not as fast as the total cross section suggests. In fact, at least 5 orders are necessary, which is consistent with the experience from nonrelativistic calculations at low energies [2]. For energies of 1 GeV and higher, the forward direction is converged at the 3rd order in  $t$ , whereas the backward angle is not as sensitive (it should be pointed out that the cross section in backward direction is about five orders of magnitude smaller than the one in forward direction). It seems accidental that the multiple scattering series converges faster at 0.5 GeV compared to 1 GeV. However, a similar finding was presented in Ref. [20], where it was observed that polarization observables for elastic proton-deuteron ( $pd$ ) scattering at 395 MeV were described better than those at 1.2 GeV, when calculating the Faddeev multiple scattering series up to the 2nd order.

### C. Breakup Scattering at Intermediate Energies

The calculation of breakup cross sections requires knowledge of the matrix element  $\langle \mathbf{k}, \mathbf{q} | U_0 | \varphi_d, \mathbf{q}_0 \rangle$  in Eq. (2.1). For details of the derivation we refer to Ref. [6] and only give the final expressions here. The five-fold differential cross section for exclusive breakup is given in the laboratory frame as [23]

$$\frac{d^5 \sigma_{br}^{lab}}{d\Omega_1 d\Omega_2 dE_1} = (2\pi)^4 \frac{E(q_0)E_d(q_0)E(q)}{2k_{lab}m_d} \frac{p_1 p_2^2}{p_2(\mathbf{E} - E(p_1)) - E(p_2)(\mathbf{P} - \mathbf{p}_1) \cdot \hat{\mathbf{p}}_2} \times E(k) \sqrt{4E^2(k) + \mathbf{q}^2} |\langle \mathbf{k}, \mathbf{q} | U_0 | \varphi_d, \mathbf{q}_0 \rangle|^2. \quad (3.5)$$

Here  $\mathbf{E}$  is the total energy of the system and  $\mathbf{P}$  its total momentum. The subscripts 1 and 2 indicate the two outgoing particles. In inclusive breakup only one of the particles is detected, and thus one of the angles in Eq. (3.5) is integrated out. This leads to the inclusive breakup cross section in the laboratory frame [24]

$$\frac{d^3 \sigma_{br}^{lab}}{d\Omega_1 dE_1} = (2\pi)^4 \frac{\mathbf{E}}{W} \frac{E(q_0)E_d(q_0)}{4k_{lab}m_d} \frac{p_1 k_a E(q)(4E^2(k_a) + \mathbf{q}^2)}{\sqrt{4E^2(k_a) + (\mathbf{P} - \mathbf{p}_1)^2}} \int d\Omega_k |\langle \mathbf{k}_a \mathbf{q} | U_0 | \varphi_d \mathbf{q}_0 \rangle|^2, \quad (3.6)$$

where  $k_a$  is determined by the condition  $W = \sqrt{4(m^2 + \mathbf{k}_a^2) + \mathbf{q}^2} + \sqrt{m^2 + \mathbf{q}^2}$ .

In Refs. [6, 23, 25] we already pointed out and demonstrated that relativistic kinematics is essential to obtain the correct position of e.g. the peak for quasi-free scattering (QFS), especially at higher energies. The difference between a nonrelativistic calculation of the breakup cross section and a relativistic one is quite large at higher energies. However one may argue that this difference is artificially large, since it is natural to use relativistic kinematics at higher energies. Therefore, here we will *not* compare to entirely nonrelativistic calculations, but rather calculations where the three-body transition amplitude has been obtained from the solution of a nonrelativistic Faddeev equation, but the transformations between the laboratory frame and the c.m. frame are Lorentz transformations. This is equivalent to comparing the relativistic and non-relativistic calculations in the center-of-momentum frame.

In addition we use the relativistic phase space factor for the cross sections. In Fig. 9 we show the inclusive breakup cross section as a function of the laboratory kinetic energy of the ejected particle at fixed angle  $\theta_1 = 24^\circ$  for different projectile kinetic energies calculated from the full solution of the relativistic Faddeev equations together with ‘nonrelativistic’ calculations using the above defined relativistic kinematics. There is still a shift of the position of the QFS peak towards lower ejectile energies, which increases with increasing projectile energy. There is also a very visible effect of the relativistic phase space factor used together with the nonrelativistic three-body transition amplitude. At 1000 MeV the size of the QFS peak is a factor of two larger compared to exact relativistic calculation. For the lower energies the 1st order calculation yields a significantly higher QFS peak compared to the full calculation, whereas for the higher energies, the peak height is almost the same for the 1st order and the full calculation.

Next we investigate in detail the convergence of the Faddeev multiple scattering series in the region of the QFS peak as a function of the projectile energy. In Fig. 10 we display calculations at selected energies from 200 to 1000 MeV. The solid line represents the solution of the relativistic Faddeev equation, whereas the other curves show the Neumann sum of the multiple scattering series containing the sum up to the order in the two-body t-matrix as indicated in the legend. For the lowest energy, 200 MeV, it is obvious that the multiple scattering series does not converge rapidly. This changes considerably as the projectile kinetic energy grows. Though the variation of the different orders is not as large anymore at 500 MeV, the multiple scattering series must still be summed up to 4th order in the QFS peak to coincide with the full result, whereas at 800 MeV already the 2nd order is almost identical with the full result, and even a 1st order calculation can be considered quite good. This trend continues as the energy grows. Of course, 1st order calculations are never able to capture the FSI peak at the maximum energy of the ejectile, nor do they describe the high energy shoulder of the QFS peak. However, our study indicates that for energies in the GeV regime it is very likely sufficient to consider only one rescattering term when studying inclusive breakup reactions in the vicinity of the QFS peak.

Finally, we also want to study the approximation suggested in Eq. (3.4), namely replacing the off-shell two-body transition amplitude embedded in the three-body Hilbert space by the half-shell one. The calculations based on the approximation of Eq. (3.4) and labeled (H) are plotted in Fig. 11 together with the exact solution. Considering only the 1st order calculation we observe a similar trend as in the differential cross section for elastic scattering, the approximation slightly underpredicts the exact result, independent of the energy under consideration. However, when this approximate two-body transition amplitude is iterated to all orders in the Faddeev equation, the deviations from the exact calculations become larger. At 800 and 1000 MeV the iteration of the exact amplitude increases the cross section in the QFS peak, whereas it decreases for the approximation with respect to the 1st order term. At 200 and 500 MeV the approximation does not only give a smaller cross section in the QFS peak but also fails to develop an FSI peak towards the maximum allowed ejectile energies. From this we conclude that Eq. (3.4) does not

provide a good approximation for inclusive breakup cross sections. Our calculations indicate that at energies 1 GeV or higher, it is important to carry out the Poincaré invariant aspects of the calculation exactly. They also indicate that it is sufficient to consider only one rescattering term to capture most features of the cross section. Although these conclusions are based on the use of a simple model two-body interaction, we conjecture that calculations based on realistic interactions will have similar characteristics.

For our study of exclusive breakup scattering in the intermediate energy regime we choose two different experimental situations where there are data available. First we consider the  $^2\text{H}(p,2p)n$  reaction at 508 MeV, where the two outgoing protons are measured for a given angle pair  $\theta_1 - \theta_2$  in the scattering plane [26]. Since the convergence of the multiple scattering series is already discussed in [23], we only want to investigate the effect of the approximations previously given in this reaction. In Fig. 12 selected angle configurations are shown. The left column of the figure shows the first order calculations and the right column the full solution of the Faddeev equation. The exact 1st order calculation is given by the dotted line in the left column and the exact full solution by the solid line in the right column. The angle combination  $\theta_1 = 41.5^\circ - \theta_2 = 41.4^\circ$  is a QFS configuration. First, we see that in a QFS configuration, the 1st order calculation is already almost identical to the full Faddeev calculation [23], whereas this is not the case for the other configurations shown. If only relativistic kinematics is considered, namely the Lorentz transformations between laboratory and c.m. frame together with the relativistic phase space factor, and a nonrelativistic three-body transition amplitude is employed, we obtain the double-dotted curve for the 1st order calculations and the dashed line for the full solution of the Faddeev calculation. Again, the QFS configuration is quite insensitive to this approximation. However, the deviation from the exact calculation is quite visible in the other two configurations shown. Finally, we also consider the approximation suggested by Eq. (3.4), which is indicated by the dash-dotted line, labeled ‘H’ in the left column (1st order calculation) and the dotted line in the right column (full solution of the Faddeev equation). Here we see that even in the QFS configuration there are already deviations of this approximation for the high energy shoulder. The approximation underpredicts the full solution. This tendency becomes stronger for the other two configurations. The interesting property of this approximation is that while it appears to be a reasonable approximation to the Faddeev kernel, the errors in the approximation increase when the equation is iterated. Thus we conclude that this approximation, though simplifying the calculation of the two-body t-matrix embedded in the three-body Hilbert space, does not seem to capture essential structures of the two-body t-matrix. The failure of this approximation, which approximates the off shell two body transition operator in the Faddeev equation with the half-shell transition operator, suggests that some care is necessary in modeling the off-shell behavior of the transition operators in more phenomenological schemes.

For breakup reaction at a slightly higher energy we consider the  $^1\text{H}(d,2p)n$  reaction at 2 GeV deuteron kinetic energy [27]. Here the two outgoing protons are measured. Energetically, this reaction would correspond to  $pd$  scattering at roughly 1 GeV and thus is within the range of the calculations presented here. In Fig. 13 we show the five-fold differential cross section as a function of the angle of the second detected proton for four different momenta of the first detected proton. The full relativistic Faddeev calculation is represented by the solid line. In order to investigate the convergence of the multiple scattering series we show the 1st order calculation as a dotted line, then successively add one (2nd order) and two (3rd order) rescattering terms to the leading order. In this reaction, the first two rescattering terms are about the same size, but have opposite sign, so that the 3rd order calculations are very close to the 1st order one. We also observe that the 3rd order calculation is already so close to the full Faddeev calculation that the Neumann series can be considered converged with three terms.

#### IV. SUMMARY AND CONCLUSION

In this work we demonstrated the feasibility of applying Poincaré invariant quantum mechanics to model three-nucleon reactions at energies up to 2 GeV. This is an important first step for studying dynamical models of strongly interacting particles in the energy range where sub-nuclear degrees of freedom are thought to be relevant. At these energies the Poincaré invariance of the theory is an essential symmetry. At lower energies non-relativistic quantum mechanical models are powerful tools for understanding the dynamics of strongly interacting nucleons. At higher energies the physics is more complicated, but one can expect that it is still dominated by a manageable number of degrees of freedom. Poincaré invariant quantum mechanics is the only alternative to quantum field theory where it is possible to realize the essential requirements of Poincaré invariance, spectral condition, and cluster properties [28]. It has the advantage that the Faddeev equation provides a mathematically well-defined method for exactly solving the strong interaction dynamics. The Faddeev equation in this framework is more complicated than the corresponding non-relativistic equation, due to the non-linear relation between the mass and energy in relativistic theories, but these difficulties can be overcome [6, 15, 29]. An important advance that allows these calculations to be extended to energies in the GeV range is the use of numerical methods based on direct integrations, rather than partial wave expansions [3, 4]. These have been successfully applied to the non-relativistic three-nucleon problem. This paper demonstrates

that they can also be successfully applied to the relativistic problem, even with its additional complications.

The model presented here involves three nucleons interacting with a spin-independent Malfliet-Tjon [30] type of interaction. It differs from more realistic interactions [8, 9, 10] in that it is spin independent and it does not give a high-precision fit to the two-body scattering data. In addition, the model is for fixed numbers of particles, not allowing pion production, which is an open channel at these energies. While these limitations must be addressed in realistic applications, the three-body Faddeev calculations presented in this paper provide a powerful framework for both testing approximations and for examining the sensitivity of scattering observables to relativistic effects.

In order to investigate relativistic effects, we treat the interaction as if it was determined by fitting the cross section obtained by solving the non-relativistic Lippmann-Schwinger equation to scattering data. When this is done with a realistic interaction the experimental differential cross section is properly transformed from the lab frame to the center of momentum frame before the fit is done. The result of this process is that the computed differential cross section agrees with the fully-relativistic experimental differential cross section in the center of momentum frame as a function of the relative momentum. Thus, even though the two-body scattering observables are computed with a non-relativistic equation, there is nothing non-relativistic about the result. At the two-body level the corresponding relativistic Lippmann-Schwinger equation must be designed to give the same scattering observables. This can be achieved by expressing the relativistic mass operator as a simple function of the non-relativistic center of momentum Hamiltonian [14, 31]. The important consequence of this is that it does not make sense to relate the relativistic and non-relativistic two-body models using  $p/m$  expansions; the prediction of the relativistic and non-relativistic two-body models are identical. Real differences in the dynamics appear when the two-body dynamical operators are used to formulate the three-body dynamics. How this must be done in the two and three-body cases is dictated, up to three-body interactions, by cluster properties. The Faddeev equation for the relativistic and non-relativistic system have identical operators forms. The permutation operators, two-body transition operators and free resolvents that are input to the Faddeev equation have different forms in the relativistic and non-relativistic equations. These differences are responsible for differences in the relativistic and non-relativistic three-body calculations.

The calculations presented in this paper have a number of consequences. The most important result is a demonstration that direct integration methods can be successfully applied to extend the energy range for converged solutions to Faddeev equations to intermediate energies. Our estimates of the number of partial waves needed for calculations at different energies suggest that it is not currently practical to extend existing partial wave calculations beyond a few hundred MeV, while in this paper we have demonstrated convergence of the direct integration methods for laboratory energies up to 2 GeV.

While our model interaction is not realistic, when we compared the results of our calculations to relativistic calculations at 200 MeV that have been performed with realistic interactions [11, 12, 13] in a partial wave basis, we found that the qualitative features of the realistic model are reproduced in our simple model, suggesting that some of the conclusions derived from our model should be applicable to models with realistic interactions.

Having a model where it is possible to perform numerically exact solutions of scattering observables in the intermediate energy range provides us with a tool to test approximations that have been used in other calculations as well as to look for observables that are sensitive to the differences between the relativistic and non-relativistic models.

One common approximation that we tested is the replacement of non-relativistic kinematic factors by the corresponding relativistic kinematic factors in a non-relativistic model. Our tests clearly illustrated a big effect, but most of it is canceled by the associated dynamical corrections. This suggests that including only kinematic corrections can actually provide large relativistic effects. Such an approach should never be used in the absence of a complete theory where relativistic effects can be rigorously estimated.

A second important set of approximations are multiple scattering approximations. These are expected to improve at higher energies, but it is important to understand in the context of models based on realistic interactions how high these energies have to be for convergence.

Our conclusion is that the convergence of the multiple scattering series is non-uniform. Even at 200 MeV our calculations show that the first-order term reproduces the total elastic cross section; for the total breakup cross section at least one more iteration is needed up to about 600 MeV. Both of these observations turn out to be misleading when one investigates the differential cross sections.

While the total elastic cross section is reproduced at 200 MeV by the first order term, the correct angular distribution requires at least five orders in the multiple scattering series. Even at 1 GeV the first order approximation is not accurate enough at forward angles.

For inclusive breakup reactions our computations show that the first order calculation does not give the right size of the quasifree peak even at 1 GeV, however for 800 MeV and above the second order term is a good approximation. For exclusive breakup the convergence of the multiple scattering series even at 1 GeV energy depends on a specific configuration.

Another type of approximation that is employed is to use on-shell transition operators with a phenomenological representation of the off-shell dependence. In our formulation of the three-body problem that off shell behavior needs



to be computed by solving a singular integral equation. It was suggested in [15] that simply replacing the off-shell two-body  $T$  by its on-shell value might be a good approximation. This was based on the observation that the difference between on and off shell Faddeev kernel is small. Our calculations show that while this does not lead to a large effect in the elastic cross section, the off-shell effects lead to non-trivial modifications when one considers the breakup cross sections. This shows that such an approximation should not be used and also suggests that phenomenological parameterizations of the off-shell behavior of the two-body amplitudes need to be carefully tested, especially for breakup reactions.

While a number of calculations have shown small relativistic effects for the three-body binding energy, non-trivial effects have already been observed in scattering observables at 200 MeV [11, 12, 13]. Our model confirms these previously observed effects and indicates that they continue into the intermediate energy region. Our calculations exhibit a number of sensitivities to relativistic effects in the breakup observables. Both the shape and size of the quasielastic peak differ from the non-relativistic quantities.

This paper demonstrates both the need for a relativistic description of few-nucleon dynamics in the intermediate energy range and shows that the problem is amenable to a numerically exact solution, using direct integration, for laboratory energies up to 2 GeV. In the future relativistic few-body calculations will be important tools for testing the validity of approximations, such as the Eikonal approximation. Obviously extensions to include spin-dependent interactions, meson channels, and interactions that are fit to higher energy data will be needed for realistic applications. The success of the calculations in this paper provide a strong motivation for continuing this program.

### Acknowledgments

This work was performed in part under the auspices of the U. S. Department of Energy, Office of Nuclear Physics, under contract No. DE-FG02-93ER40756 with Ohio University, contract No. DE-FG02-86ER40286 with the University of Iowa, and contract No. DE-AC02-06CH11357 with Argonne National Laboratory. It was also partially supported by the Helmholtz Association through funds provided to the virtual institute “Spin and strong QCD” (VH-VI-231). We thank the Ohio Supercomputer Center (OSC) for the use of their facilities under grant PHS206. Part of the numerical calculations were performed on the IBM Regatta p690+ of the NIC in Jülich, Germany.

- 
- [1] E.P. Wigner, Ann. Math. C **40**, 149 (1939).
  - [2] W. Glöckle, H. Witała, D. Hüber, H. Kamada, and J. Golak, Phys. Rep. **274**, 107 (1996).
  - [3] H. Liu, Ch. Elster, and W. Glöckle, Phys. Rev. C **72**, 054003 (2005).
  - [4] H. Liu, Ch. Elster, and W. Glöckle, Few-Body Systems **33**, 241 (2003).
  - [5] Ch. Elster, W. Schadow, A. Nogga, and W. Glöckle, Few-Body Systems **27**, 83 (1999).
  - [6] T. Lin, Ch. Elster, W. N. Polyzou and W. Glöckle, Phys. Rev. C **76**, 014010 (2007).
  - [7] F. Coester, Helv. Phys. Acta. **38**, 7 (1965).
  - [8] R.B. Wiringa, V.G.J. Stoks, R. Schiavilla, Phys. Rev. C **51**, 38 (1995).
  - [9] R. Machleidt, Phys. Rev. C **63**, 024001 (2001).
  - [10] V.G.J. Stoks, R.A.M. Klomp, C.P.F. Terheggen, and J.J.de Swart, Phys. Rev. C **49**, 2950 (1994).
  - [11] H. Witała, J. Golak, W. Glöckle, H. Kamada, Phys. Rev. C **71**, 054001 (2005).
  - [12] H. Witała, J. Golak, R. Skibiński, Phys. Lett. B **634**, 374 (2006).
  - [13] H. Witała, R. Skibiński, J. Golak, Eur. Phys. J. A **29**, 141 (2006).
  - [14] F. Coester, S.C. Pieper, F.J.D. Serduke, Phys. Rev. C **11**, 1 (1975).
  - [15] B.D. Keister and W.N. Polyzou, Phys. Rev. C **73**, 014005 (2006).
  - [16] Y. Maeda *et al.*, Phys. Rev. C **76**, 014004 (2007).
  - [17] Ch. Elster, J. H. Thomas and W. Glöckle, Few-Body System **24**, 55 (1998).
  - [18] A. Pricking, Ch. Elster, A. Gardestig and F. Hinterberger [EDDA Collaboration], arXiv:0708.3692 [nucl-th].
  - [19] The full SAID database can be accessed at <http://gwdac.phys.gwu.edu>.
  - [20] N. B. Ladygina, arXiv:0705.3149 [nucl-th].
  - [21] N. B. Ladygina and A. V. Shebeko, Eur. Phys. J. A **22**, 29 (2004).
  - [22] N. B. Ladygina and A. V. Shebeko, Few Body Syst. **33**, 49 (2003).
  - [23] T. Lin, Ch. Elster, W. N. Polyzou and W. Glöckle, arXiv:0710.4056 [nucl-th] and Physics Letters B, doi:10.1016/j.physletb.2008.01.012.
  - [24] Note that in [6] the five-fold differential breakup cross sections contain an erroneous factor of 1/3.
  - [25] Ch. Elster, T. Lin, W. N. Polyzou and W. Glöckle, arXiv:0708.3868 [nucl-th].
  - [26] V. Punjabi *et al.*, Phys. Rev. C **38**, 2728 (1988).
  - [27] J. Ero *et al.*, Phys. Rev. C **50**, 2687 (1994).
  - [28] Bert Schroer, arXiv:0711.4600 [hep-th].

- [29] H. Kamada and W. Glöckle, Phys. Lett. **B655**, 119 (2007).
- [30] R. A. Malfliet and J. A. Tjon, Nucl. Phys. **A127**, 161 (1969).
- [31] B.D. Keister and W.N. Polyzou, Advances in Nuclear Physics, Volume 20, Ed. J. W. Negele and E. W. Vogt, Plenum Press 1991.



$E_{lab}$ [GeV]	$\sigma_{op}$ [mb]	$\sigma_{tot}$ [mb]	$\sigma_{el}$ [mb]	$\sigma_{br}$ [mb]
0.1	349.4	350.6	273.4	77.2
0.2	195.1	194.6	158.6	36.0
0.5	106.2	106.8	72.2	34.6
0.8	74.2	74.5	46.6	27.9
1.0	62.3	61.8	37.7	24.1
1.2	54.6	55.3	33.0	22.3
1.5	43.7	44.9	26.0	18.9
2.0	33.0	34.1	18.9	15.2

TABLE I: The total elastic and break-up cross sections together with the total cross section extracted via the optical theorem calculated from a Malfliet-Tjon type potential as a function of the projectile laboratory kinetic energy.

$E_{lab}$ [GeV]	q $x_q$ $x_{pq}^{q0}$ $x_p$ p	q' x' $\phi''$	$\sigma_{op}$ [mb]	$\sigma_{tot}$ [mb]	$\sigma_{el}$ [mb]	$\sigma_{br}$ [mb]
1.0	50 28 12 20 50	50 20 20	0.6154E+02	0.6069E+02	0.3678E+02	0.2391E+02
1.0	50 32 12 20 50	50 20 20	0.6225E+02	0.6184E+02	0.3774E+02	0.2411E+02
1.0	50 36 12 20 50	50 20 20	0.6257E+02	0.6233E+02	0.3812E+02	0.2421E+02
1.0	50 40 12 20 50	50 20 20	0.6250E+02	0.6229E+02	0.3809E+02	0.2420E+02
1.0	50 32 12 20 50	50 20 20	0.6225E+02	0.6184E+02	0.3774E+02	0.2411E+02
1.0	50 32 12 20 50	50 24 20	0.6194E+02	0.6153E+02	0.3753E+02	0.2400E+02
1.0	50 32 12 20 50	50 28 20	0.6199E+02	0.6133E+02	0.3744E+02	0.2389E+02
1.0	50 32 12 20 50	50 32 20	0.6187E+02	0.6136E+02	0.3746E+02	0.2390E+02
1.0	50 32 12 20 50	50 20 20	0.6225E+02	0.6184E+02	0.3774E+02	0.2411E+02
1.0	50 32 16 20 50	50 20 20	0.6225E+02	0.6184E+02	0.3773E+02	0.2411E+02
1.0	50 32 12 24 50	50 20 20	0.6225E+02	0.6177E+02	0.3777E+02	0.2400E+02
1.0	50 32 12 20 50	50 20 24	0.6221E+02	0.6180E+02	0.3773E+02	0.2408E+02

TABLE II: The relativistic total elastic cross section, total breakup cross section and total cross section extracted via the optical theorem calculated from a Malfliet-Tjon type potential at 1 GeV as a function of the grid points. The double prime quantities are the integration variables.

$E_{lab}$ [GeV]	q $x_q$ $x_{pq}^0$ $x_p$ p	q' x' $\phi''$	$\theta$ [deg]	$\frac{d\sigma}{d\Omega}$ [mb/sr]	$\Delta$ [%]
1.0	50 28 12 20 50	50 20 20	0.0	0.6123E+03	
			21.8	0.1142E+01	
			62.1	0.1159E-02	
			102.3	0.4193E-02	
			151.5	0.1233E-02	
1.0	50 32 12 20 50	50 20 20	0.0	0.6266E+03	2.3
			21.8	0.1149E+01	0.6
			62.1	0.1268E-02	8.5
			102.3	0.4117E-02	1.9
			151.5	0.1233E-02	0.001
1.0	50 36 12 20 50	50 20 20	0.0	0.6318E+03	0.8
			21.8	0.1170E+01	1.8
			62.1	0.1234E-02	2.8
			102.3	0.4127E-02	0.2
			151.5	0.1230E-02	0.2
1.0	50 40 12 20 50	50 20 20	0.0	0.6319E+03	0.02
			21.8	0.1169E+01	0.1
			62.1	0.1234E-02	0.01
			102.3	0.4201E-02	1.8
			151.5	0.1234E-02	0.03

TABLE III: The relativistic elastic differential cross sections for selected scattering angles calculated at 1 GeV for a Malfliet-Tjon type potential as a function of the size of the  $x_q$ -grid. The last column indicates the percent difference with respect to the calculations for the corresponding angle in the rows above.

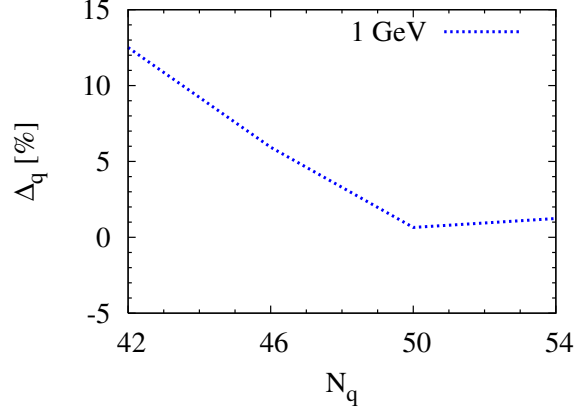


FIG. 1: (Color online) The percent error  $\Delta_q = \frac{\sigma_{op} - \sigma_{tot}}{\sigma_{op}} \times 100$  in the optical theorem as a function of the grid points in the momentum  $q$  for a calculation at 1.0 GeV.

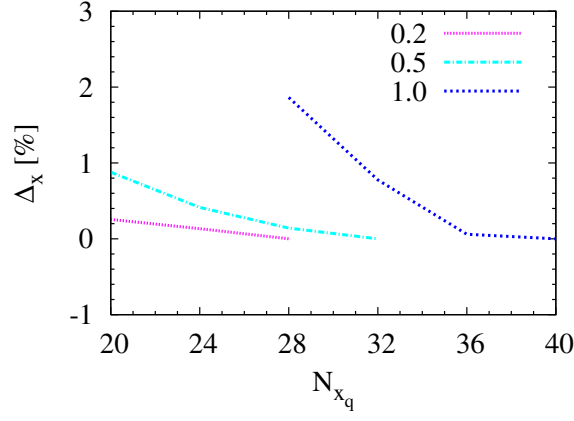


FIG. 2: (Color online) The percent error  $\Delta_x = \frac{\sigma_{op} - \sigma_{tot}}{\sigma_{op}} \times 100$  in the optical theorem as a function of the grid points in the angle grid  $x_q$ , when this grid is increased successively by 4 Gauss-Legendre points. The different curves correspond to the three different laboratory projectile energies in GeV, indicated in the legend.

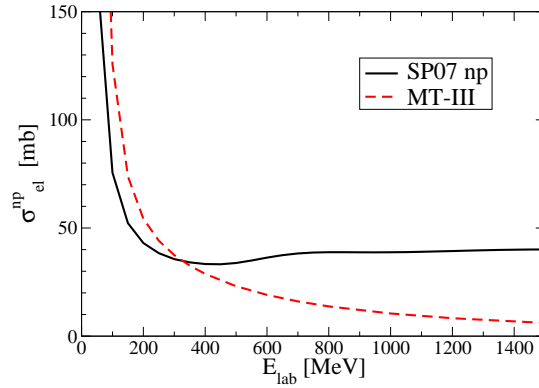


FIG. 3: (Color online) The neutron-proton differential cross section as a function of the projectile laboratory kinetic energy. The solid line represents the ‘experimental’ cross section obtained from the SAID data base [19], and the dashed line shows the two-body cross section obtained from the Malfliet-Tjon-III potential [17] used in our calculations.

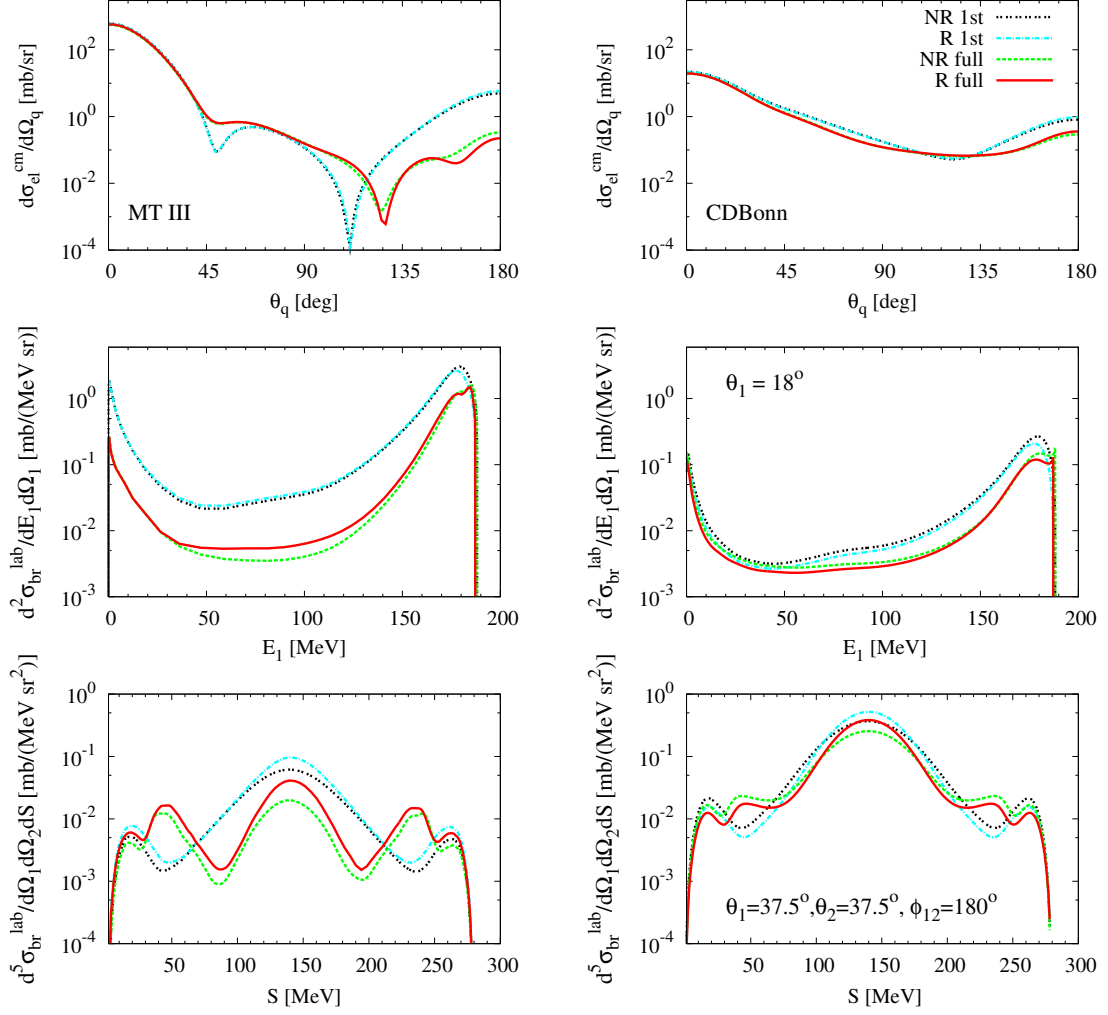


FIG. 4: (Color online) Three nucleon scattering at laboratory projectile kinetic energy  $E_{lab} = 200$  MeV. The left column shows results obtained from the Malfliet-Tjon-III potential assuming boson symmetry and no partial wave decomposition, the right column shows the corresponding realistic calculations obtained with the CD-Bonn [9] potential where partial wave decomposition is applied. The top row displays the differential cross section for elastic scattering, the middle row shows the breakup cross section for inclusive scattering for the laboratory angle  $\theta_1 = 18^\circ$  of the outgoing particle. The bottom row shows the five-fold differential for exclusive breakup reaction as a function of the arc-length  $S$ . The laboratory angles of the outgoing particles are  $\theta_1 = \theta_2 = 37^\circ$ , and  $\phi_{12} = 180^\circ$ . The fully relativistic converged Faddeev calculations are given by the solid lines (R), the corresponding nonrelativistic calculations by the long-dashed lines (NR). In addition the relativistic (dash-dot) and nonrelativistic (dotted) first order calculations are shown.

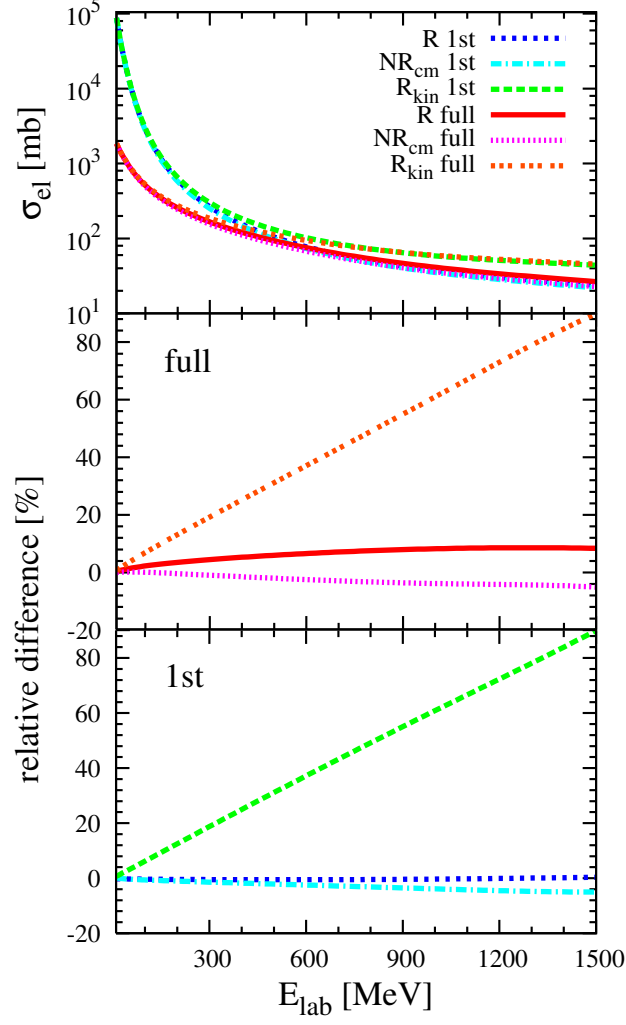


FIG. 5: (Color online) The total cross section for elastic scattering as a function of the projectile kinetic energy (top panel). The fully relativistic Faddeev calculation is shown as solid line, the corresponding first order term by the short dashed line. Calculations which only use relativistic kinematics, i.e. the Lorentz transformation between laboratory and c.m. frame together with the relativistic phase space factor (labeled  $R_{\text{kin}}$ ) are given as dotted line for a full Faddeev calculation and as short-dashed line for the first order term. Calculations which only take into account the Lorentz transformations between the laboratory and c.m. frame (labeled  $\text{NR}_{\text{cm}}$ ) are shown as dotted line for the full Faddeev calculation and as dash-dotted line for the 1st order one. The middle panel shows the relative difference between the fully relativistic Faddeev calculation and the nonrelativistic one (solid line) together with the difference to the nonrelativistic calculation if only relativistic kinematics is considered. The bottom panel shows the corresponding relative differences when only the first order term is taken into account.

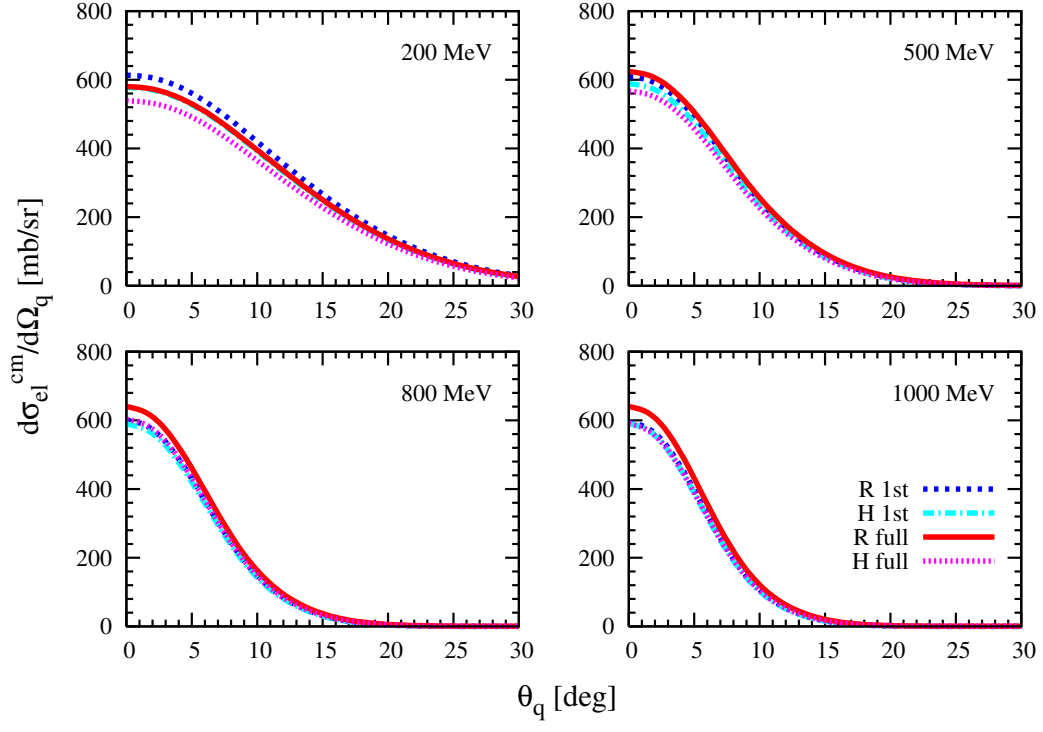


FIG. 6: (Color online) The differential cross section for elastic scattering as a function of c.m. angle  $\theta_q$  for selected laboratory kinetic energies. The converged solution of the relativistic Faddeev equation is given as solid line. The dotted line shows the converged solution of the relativistic Faddeev equation in which the fully off-shell 2N t-matrix is replaced by the half-shell t-matrix. The corresponding first order calculation are given by the short-dashed line and the dash-dotted line. For details see text.



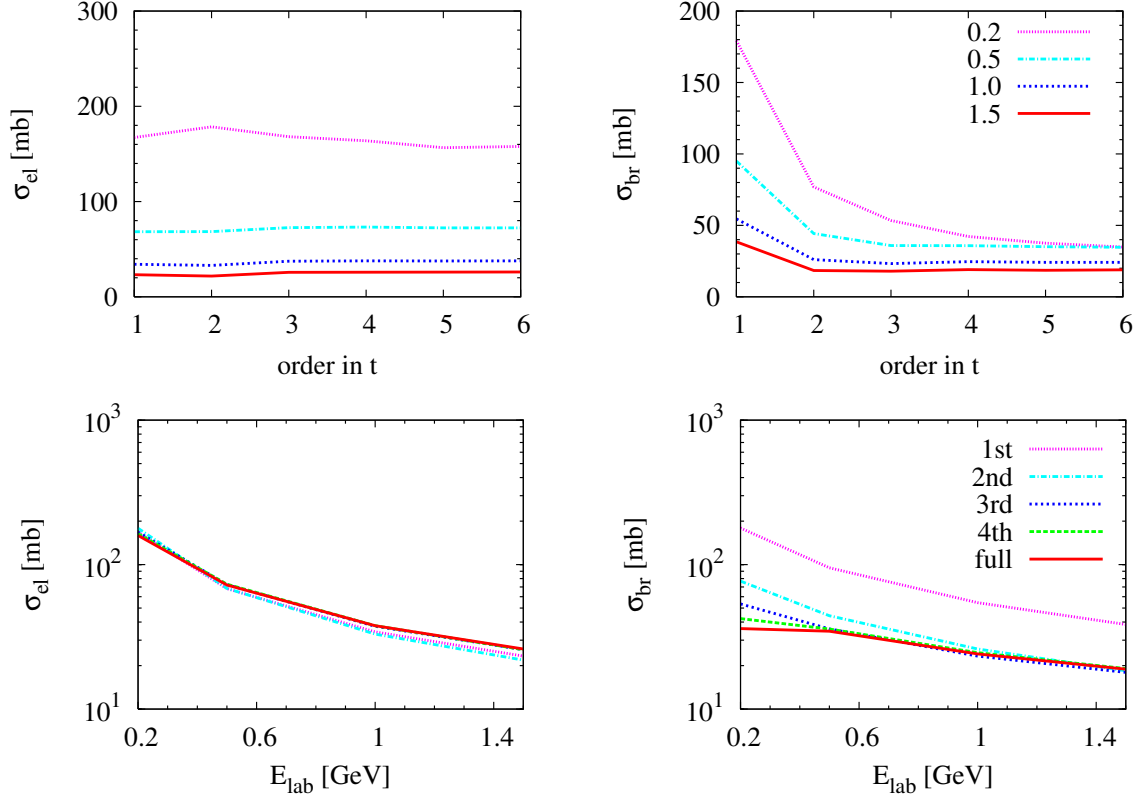


FIG. 7: (Color online) The total cross section for elastic scattering (left column) and for breakup reaction (right column). The bottom row shows both relativistic cross sections as function of the projectile laboratory kinetic energy, when starting from the first order in the Faddeev calculation successively the next 3 orders are added, together with the fully converged calculation (solid line). The top row displays the change in both total cross sections as a function of the order in the multiple scattering series for selected laboratory projectile energies (given in the legends of the top right panel in units of GeV).

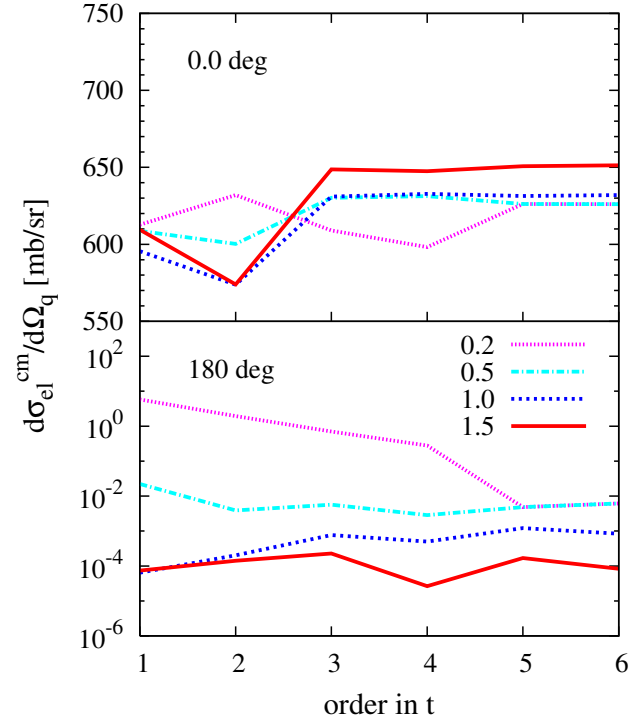


FIG. 8: (Color online) The differential cross section for elastic scattering in forward (0 deg) and backward (180 deg) direction as a function of the order in the multiple scattering series for selected projectile laboratory kinetic energies indicated in the legend in units of GeV.

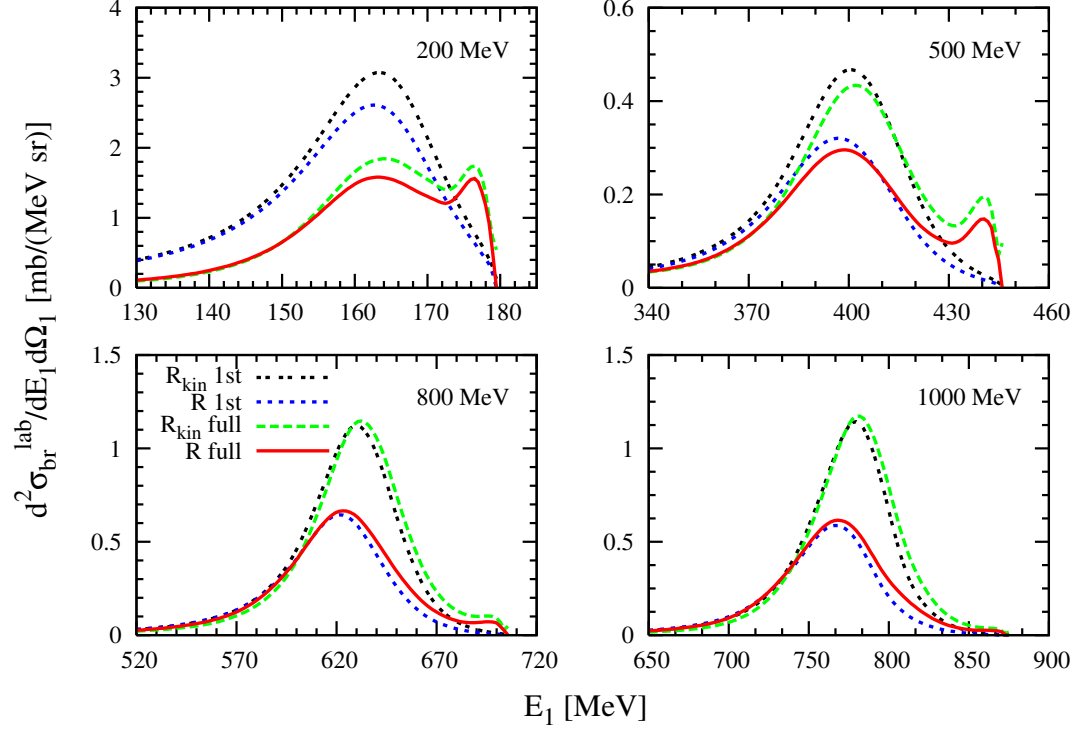


FIG. 9: (Color online) The inclusive breakup cross section as a function of the laboratory kinetic energy  $E_1$  of the emitted particle at an emission angle  $\theta_1 = 24^\circ$ . The incident laboratory kinetic energy for each cross section is indicated in each panel. The solid lines (R full) represent the converged relativistic Faddeev calculation and the dotted line the corresponding first order calculations (R 1st). The lines labeled  $R_{\text{kin}}$  correspond to calculations in which only relativistic kinematics is taken into account.

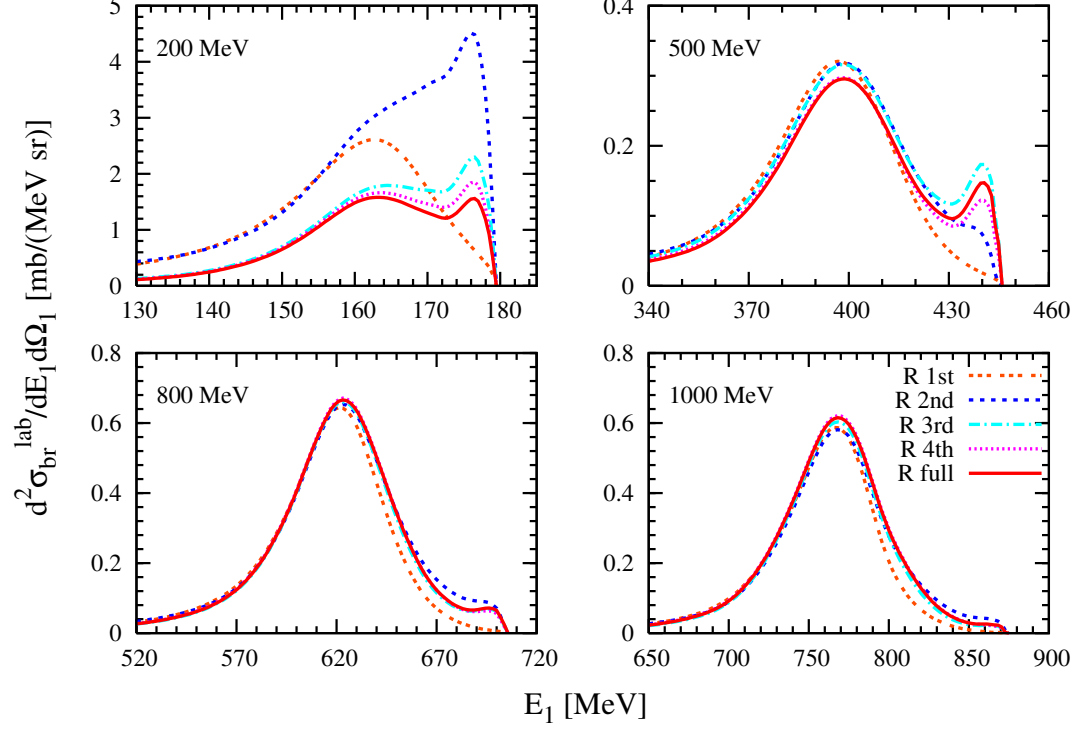


FIG. 10: (Color online) The inclusive breakup cross section as a function of the laboratory kinetic energy  $E_1$  of the emitted particle at an emission angle  $\theta_1 = 24^\circ$ . The incident laboratory kinetic energy for each cross section is indicated in each panel. The solid lines (R) represent the converged relativistic Faddeev calculation. The triple-dotted line shows the 1st order calculation, for the short dashed line the 2nd order contribution is added to the previous, for the dash-dotted line the 3rd order is added, and for the dotted line the 4th order.

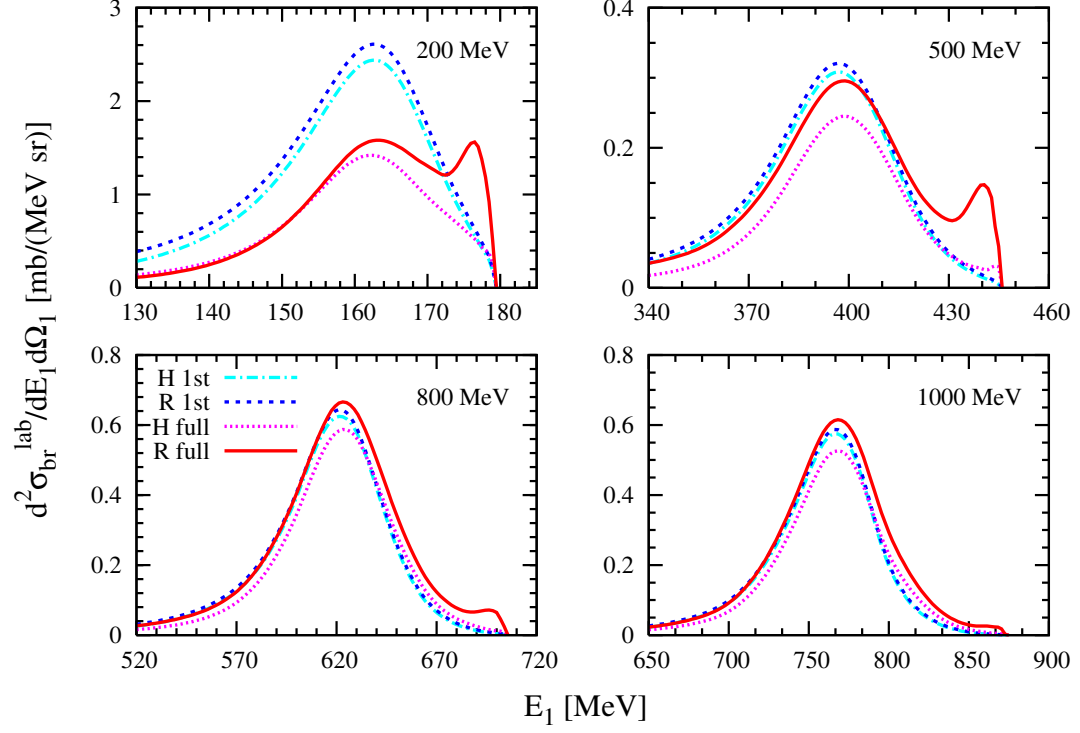


FIG. 11: (Color online) The inclusive breakup cross section as a function of the laboratory kinetic energy  $E_1$  of the emitted particle at an emission angle  $\theta_1 = 24^\circ$ . The incident laboratory kinetic energy for each cross section is indicated in each panel. The solid lines (R) represent the converged relativistic Faddeev calculation. The dotted line (H) displays the calculation in which the fully off-shell two-body t-matrix is replaced by the half-shell one. The calculations labeled 1st stand for the corresponding 1st order calculations.

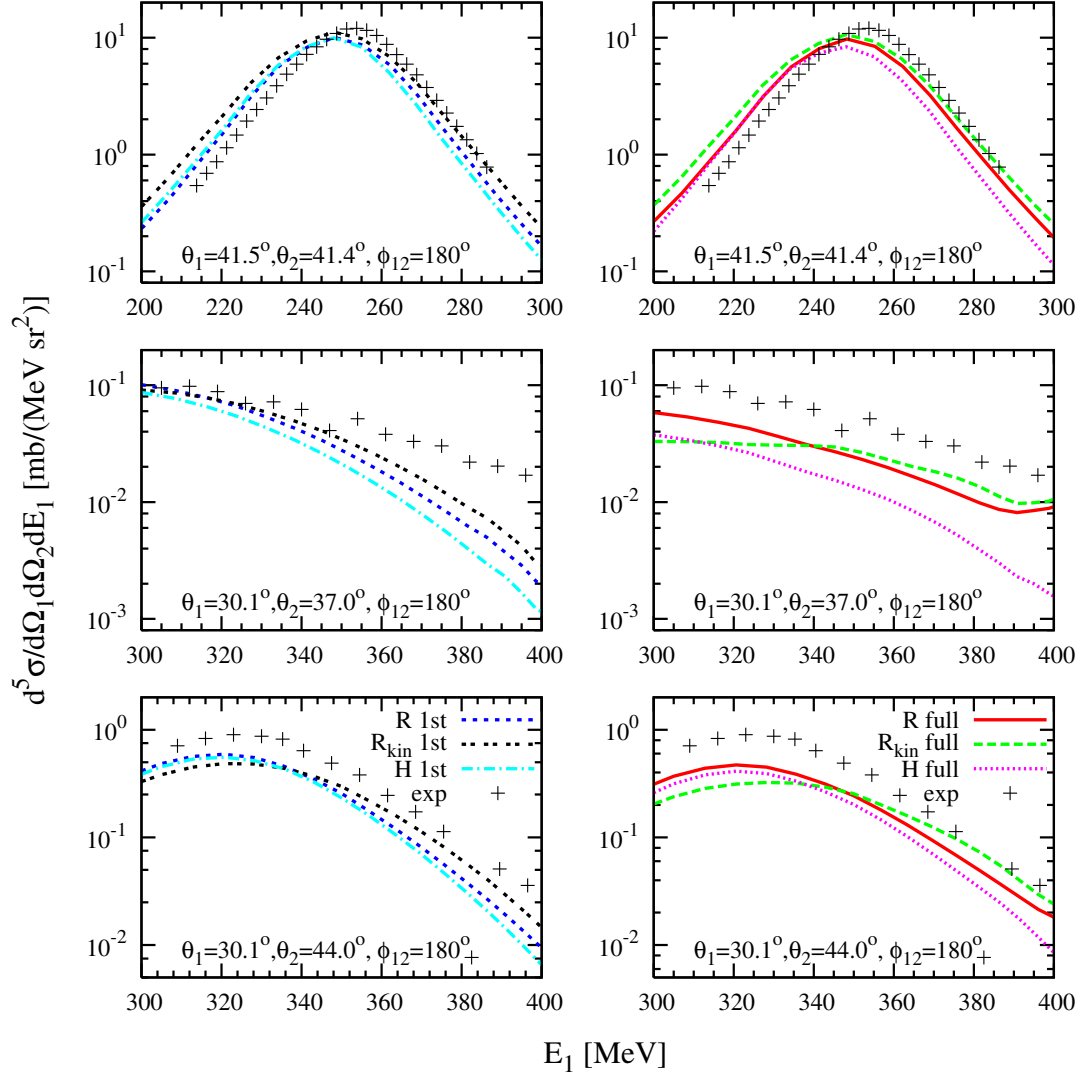


FIG. 12: (Color online) The exclusive differential cross section for the  $^2\text{H}(p,2p)n$  reaction at 508 MeV laboratory projectile energy for different proton angle pairs  $\theta_1$ - $\theta_2$  with respect to the beam axis as a function of the laboratory kinetic energy of the first detected proton. The left column represents 1st order calculation, whereas the right column gives full solution of the Faddeev equation. The curves labeled R (solid for the full Faddeev calculation and dotted for the 1st order one) represent the full relativistic calculations, whereas for the curves labeled  $R_{\text{kin}}$  (dashed in the right column and double-dotted in the left) only relativistic kinematics is taken into account (see text), and for the curves labeled H (dotted in the right column and dash-dotted in the left) the fully off-shell t-matrix is replaced by the half-shell one. The data are taken from Ref. [26].



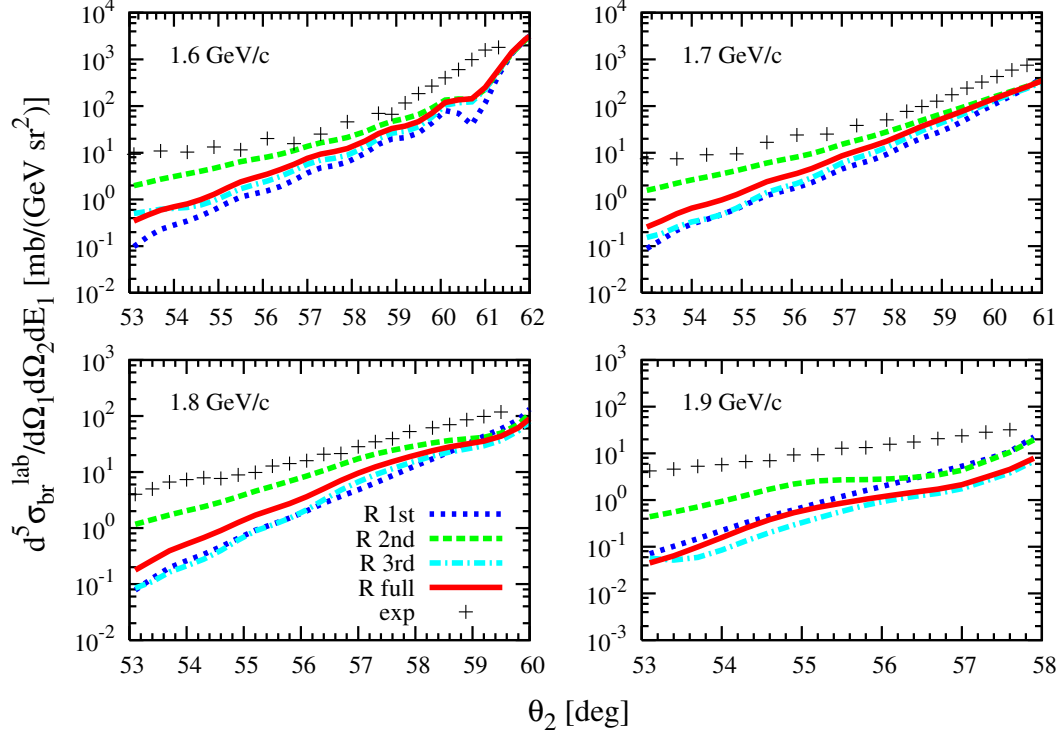


FIG. 13: (Color online) The exclusive differential cross section for the reaction  $^1\text{H}(d,2p)n$  at 2 GeV deuteron energy as a function of the angle  $\theta_2$  of the second of the outgoing protons for a fixed first proton momentum indicated in the figure. The solid line represents the solution of the full relativistic Faddeev equation. The dotted line gives the result of the first order calculation. For the dashed line the 2nd order term is added and for the dash-dotted line the 2nd and 3rd order terms are added. The data are taken from Ref. [27].